Antibacterial and Mercury Detection Abilities of Triangular Silver Nanoparticles

by

Ran An

A thesis

presented to the University of Waterloo

in fulfillment of the

thesis requirement for the degree of

Master of Applied Science

in

Chemical Engineering

Waterloo, Ontario, Canada, 2016

Author's Declaration

I hereby declare that I am the sole author of this thesis. This is a true copy of the thesis, including any required final revisions, as accepted by my examiners.

I understand that my thesis may be made electronically available to the public.

_____

Ran An

Abstract

Silver nanoparticles (AgNPs) have been studied for a long time, because of their significant application in photonics, drug delivery, biological medicine, wastewater treatment, antimicrobials, catalysis and sensors. This is due to their inherent electronic, physicochemical, biological, and visual properties, which are determined by their size, shape, composition, crystallinity, and structure. This study focuses on the synthesis of triangular silver nanoparticles, and functionalization by the biopolymer Poly-L-lysine (PLL).

$NaBH_4$ reduced triangular AgNPs were successfully synthesized, and attached by Poly-L-lysine (PLL). The morphology of AgNPs and AgNP-PLL was measured by transmission electron microscopy (TEM). The results of UV/Vis-spectroscopy, zeta-potential and dynamic light scattering (DLS) indicate that the AgNP-PLL have the property of broad-spectrum activity for both Gram-negative bacteria and Gram-positive bacteria. The bacteria tests show good results, such that when AgNP-PLL was applied to the tested bacterial strains, *E. coli* decreased 97.27 %, *P. aeroginosa* decreased 99.2%, *B. subtilis* decreased 99.14%, and *S. aureus* decreased 94.6% in 4 hours.

Toxic heavy metals have been considered to be one of the contaminants of concern in certain aqueous solutions. Polyvinylpyrrolidone (PVP) stabilized triangular AgNPs were developed for the detection of mercury (II) (Hg^{2+}). AgNPs were characterized via TEM, DLS, and UV-Vis spectrophotometry, proving that the shape of the AgNPs are triangular with an intense surface plasmon resonance, and the zeta potential results indicate that the negative surface charge of the AgNPs (-27.6 mV) can attract Hg^{2+}. In a selectivity study,

four kinds of heavy metals ions (Cr^{3+}, Pb^{2+}, Cd^{2+}, and Hg^{2+}) were applied in de-ionized (DI) water. It was shown by TEM and UV-Vis spectrophotometry that the AgNPs were specific for Hg^{2+}, which acted as a bridge to induce AgNPs aggregation. The minimum effective concentration (MEC) that could be detected by the aggregation of these AgNPs was 0.938 μM, (188.2 ng Hg^{2+}/mL water). The optimal working pH range of the AgNPs for Hg^{2+} detection was pH 7.5 to 10. From a study with tap water spiked with Hg^{2+} ions, AgNPs were slightly disturbed by ions in the tap water, but the sensitivity towards Hg^{2+} was exceptional (minimum effective concentration (MEC) is 1.25 μM).

Acknowledgements

I would first like to extend my utmost gratitude to my supervisor, Prof. William A. Anderson, for his guidance and constant support throughout my graduate career. His invaluable help of constructive comments and suggestions encourage me keep going on this research and acquired a great deal of knowledge. Furthermore, I would like to thank Dr. Shazia Tanvir, for her help and encouragement. I would also like to thank my committee member Prof. Boxin Zhao, and external committee member, Dr. Carol Moralejo for their great advices.

My special thank the portions by the Ontario Centers of Excellence and the National Science and Engineering Research Council of Canada. And sincere thanks to the support of Genemis Laboratories Inc.

Last but not least, a whole-hearted appreciation to my parents. Thank you for their inspiration and the deeply love.

Table of Contents

List of Figures

List of Tables

List of Abbreviations

AgNPs	Silver nanoparticles
AuNPs	Gold nanoparticles
Ag/AuNPs	Silver/gold nanoparticles
PLL	Poly-L-lysine
SPR	Surface plasmon resonance
SERS	Surface-enhanced Raman scattering
PVP	polyvinylpyrrolidone
PVA	Poly(vinyl acetate)
CTAB	Cetyltrimethylammonium bromide
TEM	Transmission electron microscopy
HRTEM	High resolution transmission electron microscopy
MIC	Minimum inhibitory concentration
MEC	Minimum effective concentration
CFU	Colony-forming unit
HPLC	High performance liquid chromatography
DLS	Dynamic light scattering
WHO	World Health Organisation
DI water	Deionized water
ICP	Plasma mass spectrometry
MTT	methyl thiazolyl tetrazolium
DMF	Dimethylformamide

FAAS	Flame atomic absorption spectroscopy
AAS	Atomic absorption spectroscopy
EDTA	Ethylene diamine tetra acetic acid

Chapter 1

Introduction

1.1 Motivation

Water contamination is one of the most significant contribution to human illness. Municipal wastewater and industrial wastewater are main contributors to water contamination, and pathogens and heavy metals are two of the significant pollutants in municipal and industrial wastewater. Pathogen risks have been considered as the main problem in the transportation of clean domestic drinking water. In 2008, over two million people died because of diarrheal diseases caused by polluted water (Bridle, Balharry, Gaiser, & Johnston, 2015). Heavy metals are non-degradable and persistent in the ecosystem, and they are highly toxic and can detrimentally affect both plants and animals (Ojekunle, et al., 2016) (Clarkson, Magos, & Myers, 2003) (Sharma, Katnoria, & Nagpal, 2016). Humans have used heavy metals for thousands of years, and the influence is potentially significant. For example, cadmium can cause cardiovascular diseases, cancer mortality, and damage to liver and kidneys (McFarland, Bendell-Young, Guglielmo, & Williams, 2002); lead can cause memory loss, irritability, anemia, and muscle paralysis, particular for children (Godwin, 2001); mercury is well known for its highly cell toxicity which can cause serious damage to the central nervous system (Clarkson, Magos, & Myers, 2003) (Carvalho, Chew, Hashemy, Lu, & Holmgren, 2008). Because of the food chain systems, heavy metals will eventually accumulate inside the human body (Johnson, Wallace, Cashman, Granados, & Kent, 2008) (Mingorancea, Valdés, & Oliva, 2007) (Dai, et al., 2012).

Therefore, novel techniques are desired for the detection and prevention of those types of contaminations.

In recent years, nanotechnology has been used in many areas, due to the advantages of the relatively large surface area achieved with nanoparticles (Riu, Maroto, & Rius, 2006) (Huang & Choi, 2007). In the field of metal nanomaterials, noble metals, like silver and gold nanoparticles, have been widely used. With the development of nanoscientific technologies, silver and gold nanoparticle production is not limited to spherical shapes but to triangular and other shapes as well. Triangular shaped nanoparticles are easy to manipulate and have an intense surface plasmon (Sun & Xia, 2002) (Shi & Ma, 2010), which can be the basis for various applications.

Silver ions have been widely known for their antibacterial and antifungal properties (Crabtree, et al., 2003), because they are highly toxic to microbes, but have a low toxicity to mammals (Zhao & Stevens, 1998). In addition, silver nanoparticles (AgNPs) are able to seriously damage the structure of infectious microbes and are active against a broad-spectrum of Gram-positive and Gram-negative bacteria, including antibiotics resistant bacteria (Burrell, Heggers, Davis, & Wrigh, 1999) (Rai, Yadav, & Gade, 2009). Based on the property of different shape and size silver and gold nanoparticles (Ag/AuNPs) have different colors, and Ag/AuNPs could be used as colorimetric detection sensors for heavy metals. Using Ag/AuNPs for heavy metal detection could avoid complicated instrumentation and sample preparation (Lee, Han, & Mirkin, 2007) (Darbha, et al., 2008) (Li, Wieckowska, & Willner, 2008).

1.2 Research Objectives

The first objective of this thesis was to construct and acquire a qualitative understanding of the anti-bacterial properties of Poly-L-lysine (PLL) developed triangular silver nanoparticles by using gram-positive bacteria and gram-negative bacteria (Chapter 3).

The second objective was to investigate the triangular silver nanoparticles (AgNPs) as a heavy metal probe (Chapter 4) with mercury as the main target, and establish a detection protocol. In additional, the minimum effective concentration (MEC) was investigated in this study.

Finally, a minor objective was to study the application of using silver nanoparticles (AgNPs) and gold nanoparticles (AuNPs) as a biosensor, and in the development of a lateral flow assay for bacterial detection (Appendix).

Chapter 2

Literature review

2.1 Silver and Gold Nanoparticles

Noble metal nanoparticles have been studied for a long time, because of their significant application in photonics, drug delivery, biological medicine, wastewater treatment, antimicrobials, catalysis, and sensors. Their success in these applications is due to their inherent electronic, physicochemical, biological, and visual properties, which are determined by their size, shape, composition, crystallinity, and structure (Sun & Xia, 2002) (Xia, Xiong, Lim, & Skrabalak, 2008). Among the metal nanoparticles, silver nanoparticles (AgNPs) and gold nanoparticles (AuNPs) are the most widely used.

2.1.1 Synthesis of Silver nanoparticles

Silver nanoparticles can be synthesized with various methods. But there are mainly two categories, chemical and physical methods. In these two categories, the chemical method is the most commonly used. Lee and Meisel used the approach of reducing Ag ion by elemental hydrogen, sodium borohydride, and sodium citrate in 1982. They found that the AgNPs reduced by elemental hydrogen and sodium citrate had a brown color, producing an absorption band with a peak centred at approximately 400 nm; whereas the AgNPs reduced by sodium borohydride were a green-yellow color with an absorption peak centred around 420 nm (Lee & Meisel, 1982). In1999, Neil Shirtcliffe et al. synthesized larger sized particle AgNPs (from 40 nm to 80 nm) by development of the borohydride method. They grew AgNPs using a silver sol, which was

synthesized via the citrate method of Lee, and several factors that may affect the size of the AgNPs were considered in their experiments, namely temperature, mixing rate, and the ratio between silver and borohydride (Shirtcliffe, Nickel, & Schneider, 1999). They also found that the AgNPs produced using the above method could be used as nuclei to grow even larger AgNPs by using ascorbate as a reducing agent (Shirtcliffe, Nickel, & Schneider, 1999). AgNPs also can be reduced by hydrazine in a certain pH range (pH 7-10.5), and the AgNPs could keep a spherical shape with a particle diameter range between 40-70 nm (Nickel, Castell, Poppl, & Schneider, 2000). Well-defined clean AgNPs were synthesized by using hydrogen, ultrapure water, and silver oxide in 2004, where hexagonal shaped AgNPs were formed and the particle size was well defined (Evanoff & Chumanov, 2004). With this method, AgNPs could be produced in a scalable way such that they were stable for a long term (Evanoff & Chumanov, 2004). In this experiment no stabilizer had been used, allowing for the synthesis of AgNPs of any diameter from 15 nm to 200 nm (Evanoff & Chumanov, 2004). From previous research, the most commonly used chemical reducing agents are borohydride, citrate, ascorbate, and elemental hydrogen.

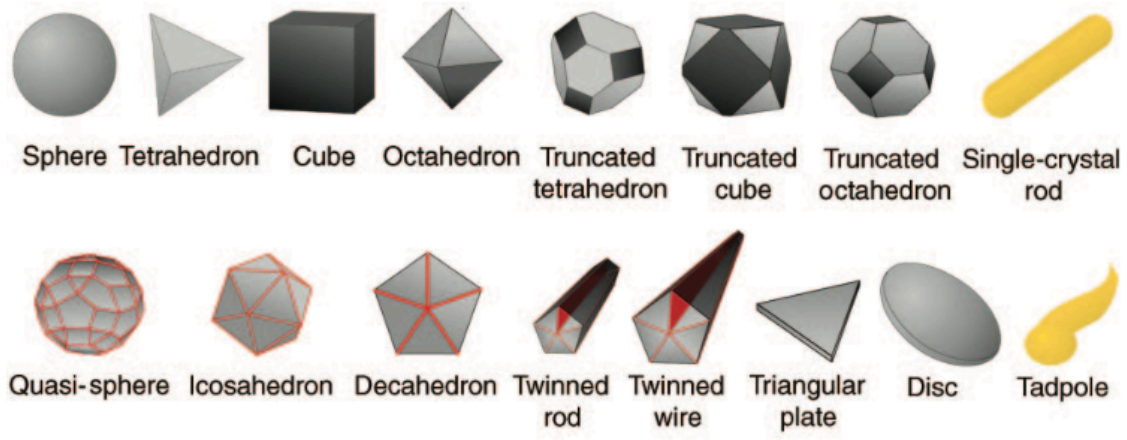

Figure 2.1 Nanostructure shapes. First row is single crystals, second row is particles with twin defects or stacking faults (from (Xia & Halas, 2005)).

With the development of chemical synthesis, researchers found AgNPs can be formed in various shapes, like tetrahedrons, cubes, rods, octahedrons, truncated octahedrons (Figure 2.1), and others. The shape diversification of silver nanoparticles results in a high surface plasmon resonance (SPR). Surface plasmon resonance (SPR) is a special property of metals, meaning they could be excited by light energy (Pattnaik, 2005). In the past decades, a number of applications based on surface plasmon resonance have been studied, especially for surface enhanced Raman scattering (SERS), SPR absorption for photothermal therapy, and biosensing (Jain, Huang, El-Sayed, & El-Sayed, 2007). Triangular silver nanoparticles were widely used in recent years, due to their apparent color change based on size difference (Shi & Ma, 2010) (Silva, Saade, Farias, & Falcão, 2013) (Chun, 2009).

Because the chemical reducing agents may cause environmentally issues, green methods for synthesis of AgNPs have also been developed. For example, polysaccharides from starch and glycogen have been used for AgNPs synthesis. Starch was used as a capping agent, and β-D-glucose was used as a nontoxic reducing agent. Ag ion was mixed with starch and glucose with slow heating and stirring (Raveendran, Fu, & Wallen, 2003). In this method, the stabilization agent was starch that because starch is environmentally friendly, and the binding between starch and AgNPs is relatively weak and can be easily reversible (Raveendran, Fu, & Wallen, 2003). The synthesized AgNPs were spherically shaped and produced a yellow color with average particle size around 5.3 nm (Raveendran, Fu, & Wallen, 2003). This method avoided the highly toxic reducing agents and used an environmentally benign material, resulting in AgNPs that were stable and well dispersed in water (Raveendran, Fu, & Wallen, 2003). In the following year,

Haizhen Huang et al. reported a similar method, where polysaccharide from heparin was used as both a stabilizing and reducing agent, and the sulfonate groups in heparin could accelerate the formation of AgNPs (Huang & Yang, 2004). Some others environmentally friendly reducing agents such as extracts from bio-organisms also served as capping agents, like enzyme/proteins, amino acid, vitamins (Li, et al., 2007). For example, single crystalline AgNPs were synthesized by an extract of the unicellular green alga *Chlorella vulgaris* at room temperature, and in this reaction, proteins were involved and served as reducing agents and shape controllers (Xie, Lee, Wang, & Ting, 2007).

Physical methods can also successfully synthesize AgNPs, and these mainly use irradiation. For example, a well-defined size and shape distribution of AgNPs was formed by laser irradiation directly applied to aqueous Ag salt and surfactant without reducing agents (Abid, Wark, Brevet, & Girault, 2002). In addition, a photo-sensitization synthesis technique for producing AgNPs employed benzophenone (Eustis, et al., 2005). Both a laser and mercury lamp were involved in this study, and the results showed that a short time irradiation with low laser intensity made AgNPs with a size around 20 nm, while high laser intensity gave AgNPs around 5nm (Eustis, et al., 2005). In other research, visible light irradiation could also synthesize AgNPs by employing thionine as a sensitizing dye, and the AgNPs size increased with the time of photolysis (Sudeep & Kamat, 2005).

Microwave irradiation has been applied to AgNPs synthesis procedures in the last decade. Uniform AgNPs could be produced in a solution of sodium carboxymethyl cellulose and $AgNO_3$ with microwave irradiation, and these AgNPs were stable for two months at room temperature (Chena, Wang, Zhang, & Jin, 2008). A three minutes rapid method of AgNPs synthesis was carried out where a mixture of nanorods, nanowires, spherical, cubic, and triangular AgNPs was

obtained by reducing Ag ions in ethylene glycol, $H_2[PtCl_6]$ and PVP (Tsuji, et al., 2008). Ionizing radiation synthesis and radiolysis have been employed in the AgNPs production, where methanol was used as the solvent in the process of ionizing radiation synthesis, resulting in a particles size of around 10 nm (Henglein, 1993). Radiolysis of AgNPs, for example, AgNPs grown on silica aerogel were formed via gamma radiolysis (Ramnani, Biswal, & Sabharwal, 2007). The optimal pH range for the AgNPs production is pH 2-9, and for pH over 9 AgNPs aggregation occurred (Ramnani, Biswal, & Sabharwal, 2007). Table 2.1 summarizes the common methods of AgNPs synthesis with their properties.

Table 2.1 Common methods of AgNPs synthesis with their properties.

Methods	**Reducing agents/tools**	**Capping agents**	**Properties**	**Reference**
Chemical method	Sodium borohydride, sodium citrate, ascorbate acid, and elemental hydrogen	PVP PVA Most of them are bared AgNPs	Size: 10-200 nm Most of them are spherical shape Absorption around 400 nm Some are triangular shape, surface enhance Raman scattering	(Evanoff & Chumanov, 2004) (Nickel, Castell, Poppl, & Schneider, 2000) (Shirtcliffe, Nickel, & Schneider, 1999) (Lee & Meisel, 1982) (Shi & Ma, 2010)

				(Jain, Huang, El-Sayed, & El-Sayed, 2007)
Biological method	Enzymes/proteins, amino acids, polysaccharides, and vitamins	Glutathione, polysaccharide, etc.	Green synthesis, Environmental friendly	(Xie, Lee, Wang, & Ting, 2007) (Huang & Yang, 2004) (Raveendran, Fu, & Wallen, 2003) (Li, et al., 2007)
Physical method	Laser irradiation, photo-sensitization synthetic technique, photolysis	N/A	No reducing agents in solution. Rapid reaction. Process could be controlled	(Abid, Wark, Brevet, & Girault, 2002) (Chena, Wang, Zhang, & Jin, 2008) (Tsuji, et al., 2008) (Sudeep & Kamat, 2005) (Eustis, et al., 2005) (Henglein, 1993)

2.1.2 Synthesis of Gold nanoparticles

Gold nanoparticles (AuNPs) are also being widely used in drug delivery, biosensing and therapy, because of their strong biological compatibility, high surface plasmon resonance, and anti-cancer properties (PATRA, PANDA, & DHAL, 2015). The approaches for synthesis of AuNPs are similar to those for silver. There are chemical approaches, green approaches, and photochemical approaches, etc.

Typically, AuNPs were prepared by the citrate reduction of $HAuCl_4$ (Turkevich, Stevenson, & Hillier, 1951). Since the citrate reduction method was carried out by John Turkevich et al., a range of research based on this method has been studied. The size of sodium citrate reduced AuNPs can be controlled by pH, with studies showing that using a pH range between 6.2 and 6.5 with this approach, AuNPs were well dispersed and had a uniform size and shape (Ji, et al., 2007). Self-assembled AuNPs were formed via the citrate reduction method, where 5 nm AuNPs can self-assembled to form chain-like nanowires with branches, and finally to become a nanowire network (Pong, et al., 2007). A developed citrated reduction method with Ag^+ ions in boiling water can produce considerably uniform and well-dispersed AgNPs (Figure 2.2) (Xia, Ba, Hartmann, & Wang, 2010).

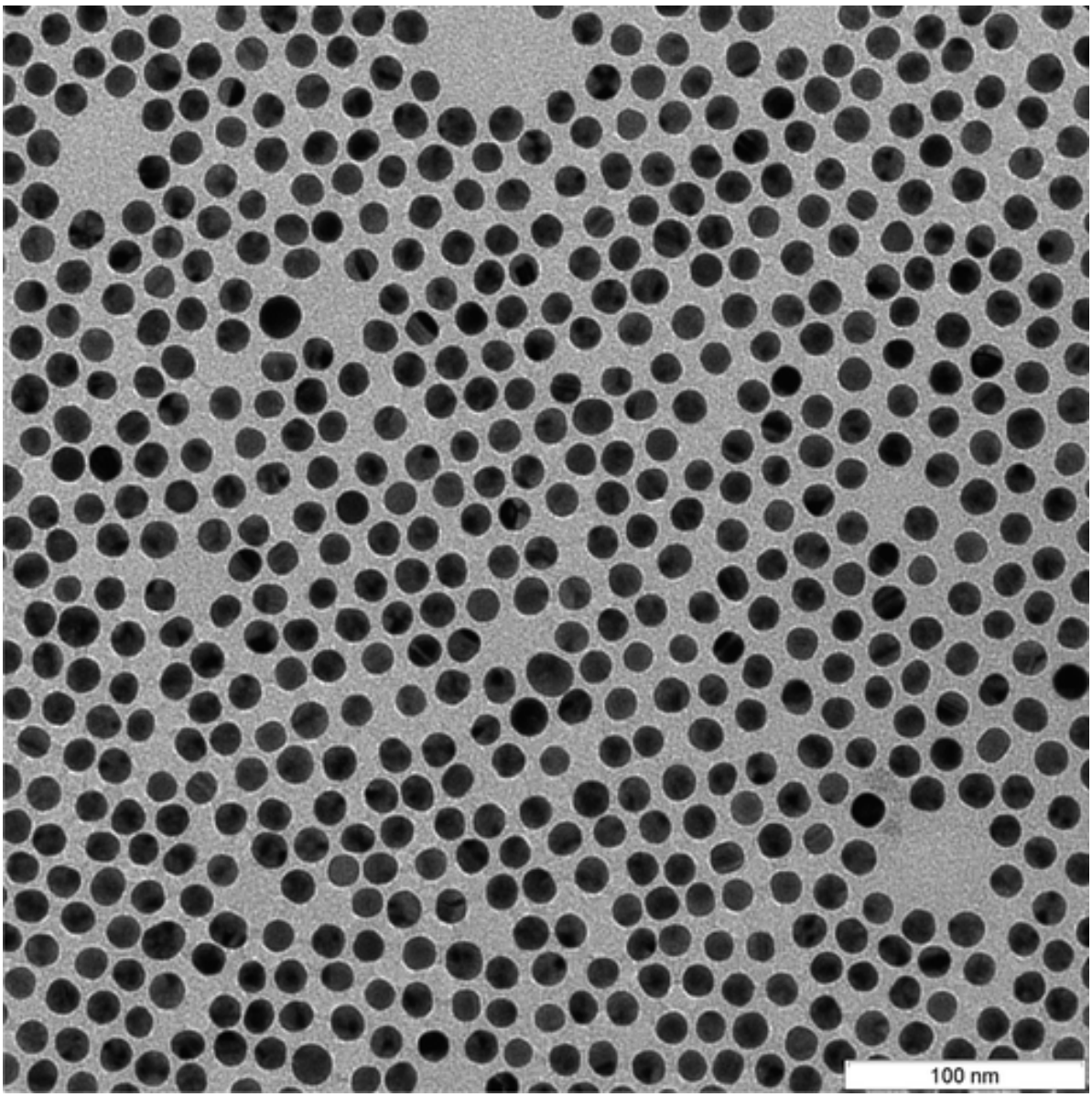

Figure 2.2 Well-dispersed and uniform size AuNPs produced via citrate reduction method (from (Xia, Ba, Hartmann, & Wang, 2010))

Some researchers also used sodium borohydride to prepare a gold seed around 3.5 nm, and AuNPs can then be prepared based on gold seed (Jana, Gearheart, & Murphy, 2001). Here, tri-sodium citrate served as a capping reagent, and cetyltrimethylammonium bromide (CTAB) was

used to stabilize the particles (Jana, Gearheart, & Murphy, 2001). Surface coating of thiol AuNPs (1-3 nm) were synthesized with a water-toluene phase change method, which is reduced by sodium borohydride in the presence of alkanethiol (Brust, Walker, Bethell, Schiffrin, & Whyman, 1994). Novel thiol capped AuNPs were produced by M. K. Corbierre et al. in 2005, and compared with the conventional method (Brust, Walker, Bethell, Schiffrin, & Whyman, 1994), it avoided the potential insolubility of AuNPs (Corbierre & Lennox, 2005). Chemical reduction combined with a photochemical approach gave a quick way to produce AuNPs. For example, for ascorbic acid combined with ultraviolet photoirradiation reduction of AuNPs, the shape could change with the reaction progress (Niidome, Nishioka, Kawasaki, & Yamada, 2003). In summary, chemical methods to synthesize AuNPs commonly include a reducing agent, like sodium citrate, sodium or potassium borohydride, ascorbic acid, hydrazine, or dimethyl formamide.

However, chemical methods always bring potential environment problems. Therefore, some researchers studied green biosynthetic methods with plant extracts and microbes for reduction AuNPs. For example, *Avena sativa* biomass reduced Au^{3+} in aqueous solutions and the size of AuNPs was controlled by pH, where large particles were formed at pH 2 and as the pH increased the particles size decreased (Armendariz, et al., 2004). But in this study, the shape of AuNPs was irregular such that tetrahedral, decahedral, hexagonal, icosahedral multitwinned, and rod shape were all found in the HRTEM images (Armendariz, et al., 2004). Marine sponge *Acanthella elongata* extract was added to Au^{3+} and formed pink-ruby red color AuNPs, with the size of particles ranging from 7-20 nm with most of them approximately 15 nm (Inbakandan, Venkatesan, & Khan, 2010).

Bacteria are also one kind of bioreductant, where the extracellular method is the most common because it is a very simple procedure. Typically, micro-organisms were centrifuged after culturing for 1-2 days, and this was then added to gold salt solution (Ahmed, Annu, Ikram, & Yudha S., 2016). *Streptomyces sp. MBRC-82* reduction of $HAuCl_4 \cdot 3H_2O$ solution gave a spherical shape of AuNPs of around 40 nm (Manivasagan, et al., 2015). A summary of some previous studies is shown in Table 2.2.

Table 2.2 List of recent years research of biosynthesis of gold nanoparticles.

Bioreductants	**AuNPs size**	**AuNPs shape**	**Reference**
Avena sativa	5-85 nm	Spherical, triangular, rod	(Armendariz, et al., 2004)
Acanthella elongata	7-20 nm	Spherical	(Inbakandan, Venkatesan, & Khan, 2010)
Coriander leaf	6-58 nm	Spherical, triangular	(Narayanan & Sakthivel, 2008)
Cymbopogon citratus	2-100 nm	Spherical, triangular	(Murugan, et al., 2015)
Hovenia dulcis	20 nm	Spherical, hexagonal	(Basavegowda, Idhayadhulla, & Lee, 2014)

Lamiaceae	150 nm	Spherical	(MubarakAli, Thajuddina, Jeganathan, & Gunasekaran, 2011)
Abelmoschus esculentus	62 nm	Spherical	(Jayaseelan, Ramkumar, Rahuman, & Perumal, 2013)
Trianthema decandra L.	37.7-79.9 nm	Spherical	(Geethalakshmi & L., 2013)
Lentinus edodes	5-50 nm	Spherical	(Vetchinkina, Loshchinina, Burov, Dykman, & Nikitina, 2014)
Galaxaura elongate	3.85-77.13 nm	Spherical	(Abdel-Raouf, Al-Enazib, & Ibraheem, 2013)
Olive leaf	50-100 nm	Triangular	(Khalil, Ismail, & El-Magdoub, 2012)
Gymnocladus	4.5-22.5 nm	Planar	(Tamuly, Hazarika, &

assamicus			Bordoloi, 2013)
Punica granatum	70 nm	Spherical	(Ganeshkumar, Sathishkumar, Ponrasu, Girija, & Suguna, 2013)
Cassia auriculata	15-25 nm	Spherical, hexagonal, triangular	(Kumar, et al., 2011)
Nerium oleander leaf	10 nm	Spherical	(Tahir, et al., 2015)
Rose hybrida	10 nm	Spherical, triangular, hexagonal	(Noruzi, Zare, Khoshnevisan, & Davoodi, 2011)
Prasiola crispa	5-25 nm	Spherical	(Sharma, Dhar, Hazra, & Gogoi, 2014)
Pleurotus sapidus	15-100 nm	Spherical	(Sarkar, Kalyan, Laskar, Chattopadhyay, & Acharya, 2013)
Mango peel	4-21 nm	Spherical	(Yang, Li, & Hao,

			2014)
Krishna tulsi leaf	30 nm	Hexagonal	(Philip & Unni, 2011)
Tagetes patula	45 nm	Spherical	(Ateeq, et al., 2015)
Dysosma pleiantha	127 nm	Spherical	(Karuppaiya, et al., 2013)
Curcuma pseudomontana	20 nm	Spherical, cubic	(Muniyappan & Nagarajan, 2014)
Streptomyces sp. MBRC-82	20-80 nm	Spherical	(Manivasagan, et al., 2015)
Micrococcus luteus	6 nm and 50 nm	Spherical	(Arunkumar, Thanalakshmi, Kumar, & Premkumar, 2013)
Staphylococcus epidermidis	20-25 nm	Spherical	(Srinath & Rai, 2015)
Pseudomonas aeruginosa	15-30 nm	Spherical	(Husseiny, El-Aziz, Badr, & Mahmoud, 2007)
Inonotus obliquus	23 nm	Spherical, triangular,	(Lee, Nagajyothi,

		hexagonal	Sreekanth, & Park, 2015)
Rhodopseudomonas capsulate	10-20 nm	Spherical	(He, et al., 2007)
Shewanella oneidensis	2-50 nm	Spherical	(Suresh, et al., 2011)
Geobacillus stearothermophilus	5-8 nm	Spherical	(Fayaz, Girilal, Rahman, Venkatesan, & Kalaichelvan, 2011)
Brevibacterium casei	10-50 nm	Spherical	(Kalishwaralal, et al., 2010)

In 1995, Kunio Esumi et al. used cationic micelles as templates to synthesize AuNPs with UV irradiation of 253.7 nm light, and they produced rod shape AuNPs by increasing the irradiation time (Esumi, Matsuhisa, & Torigoe, 1995). Morphology controlled AuNPs were produced by a slow UV irradiation method, where the key factors that controlled the shape were the concentration of Au cation and the irradiation time (Zhou, Wang, Zhu, & Chen, 1999). Large AuNPs (20-110 nm) can be formed based on an Au seed (5-20 nm), which was produced by UV irradiation (Sau, Pal, Jana, Wang, & Pal, 2001). Hydrophobic AuNPs were formed by

microwave irradiation combined with ethanol reduction (Shena, Du, Hua, & Yang, 2006). Kenji Okitsu et al. used sonochemical methods to synthesize gold nanorod particles by ultrasonic irradiation, and they evaluated the size of aspect ratio change of AuNPs with different pH value, where the aspect ratio of AuNPs increased with the pH value decreasing in solution (Okitsu, Sharyo, & Nishimura, 2009).

2.2 Application of silver/gold nanoparticles

2.2.1 Detection and Anti-microbial

Since an increasing number of new bacterial strains are resistant to current antibiotics, this has become a significant issue for public health. Thus, development of new types of bactericides is important. Silver has been known to exhibit a strong toxicity to a wide range of micro-organisms (Liau, Read, Pugh, Furr, & Russell, 1997), and silver based compounds have been used widely in the antimicrobial area (Gupta & Silver, 1998). Table 2.3 lists a simple summary of selected AgNPs antibacterial research in recent years.

Table 2.3 List of recent years research of AgNPs antibacterial applications.

Type of AgNPs	**Bacterial strains**	**Antibacterial Properties**	**Reference**
13.4 nm spherical AgNPs	Yeast, E. coli, S. aureus	MIC of yeast was 6.6 nM MIC of E. coli was	(Kim, et al., 2007)

		over 3.3 nM MIC of S. aureus was over 33 nM	
16 nm AgNPs	E. coli	Completely inhibition of E. coli was 60 µg/mL	(Raffi, et al., 2008)
26 nm AgNPs	Standard strains, Strains from clinical material	MIC was 1.69- 13.5 µg/mL	(Kvitek, et al., 2008)
10 nm AgNPs	E. coli, S. aureus, L. mesenteroides	Growth inhibition of E. coli and S. aureus was 5 µg/mL Growth inhibition of L. mesenteroides was 2.5 µg/mL	(Vertelov, Krutyakov, Efremenkova, Olenin, & Lisichkin, 2008)
HPAMAM-N(CH_3)$_2$ stabilized 1.4-7.1 nm AgNPs	E. coli, S. aureus, B. subtilis,	Antibacterial activity increases as AgNPs size decrease	(Zhang, Peng, Huang, Zhou, & Yan, 2008)

	K. mobilis		
PAMAM-AgNPs	S. aureus, P. aeruginosa, E. coli	Antibacterial activity was higher than silver ion	(Balogh, Swanson, Tomalia, Hagnauer, & McManus, 2001)
Ag-zeolite	E. coli	CFU reduce by 7 log units in 5 min	(Inoue, et al., 2002)
Ag-Zn-zeolite	E. coli, S. aureus, P. aeruginosa	MIC of E. coli was 78 μg/mL (base on Ag) MIC of S. aureus and P. aeruginosa were 39 μg/mL (base on Ag)	(Cowan, Abshire, Houk, & Evans, 2003)

In addition, in the report of Kvitek et al. AgNPs were modified by two surfactants, Tween 80 and PVP 360, and the antibacterial activity of modified AgNPs was increased for several bacterial strains (Kvitek, et al., 2008). For example, the MIC of PVP 360 modified AgNPs was decreased to 1.69 μg/mL for *P. aeruginosa* and *S. aureus* MRSA, and it was decreased to 3.38 μg/mL for *E. faecium* VRE (Kvitek, et al., 2008).

AgNPs do not only work for bacteria, but they also can inactivate other micro-organisms. HPAMAM-N$(CH_3)_2$-AgNPs inhibited the growth of the fungi *A. niger* and *P. citrunum*, and PAMAM-AgNPs also can inhibit the growth of *A. niger* (Zhang, Peng, Huang, Zhou, & Yan,

2008) (Balogh, Swanson, Tomalia, Hagnauer, & McManus, 2001). While in another study, 3 nm spherical AgNPs had a MIC of 1-4 μg/mL for inhibition of *T. mentagrophytes* and 2-4 μg/mL for *C. albicans* (Kim, et al., 2008). Virus inactivation has also been studied in the last decade. For example, AgNPs could inhibit the in vitro production of HBV RNA (Lu, et al., 2008). Additionally, AgNPs ranging in size from 1 to 10 nm were able to inhibit HIV-1 virus via binding to the host cells (Elechiguerra, et al., 2005). Table 2.4 shows a summary of results of recent literatures.

Table 2.4 List of recent years research of AgNPs antifungial and antiviral applications.

AgNPs	**Fungi/Viruses**	**Properties**	**Reference**
m AgNPs	Fungi: A. niger S. cerevisiae	MIC of A. niger and S. cerevisiae were 5 μg/mL	(Vertelov, Krutyakov, Efremenkova, Olenin, & Lisichkin, 2008)
1.4-7.1 nm HPAMAM-N(CH_3)$_2$-AgNPs	Fungi: A. niger P. citrinum	Inhibition zones were formed around AgNPs spots in agar plates	(Zhang, Peng, Huang, Zhou, & Yan, 2008)
3 nm AgNPs	Fungi:	MIC of T. mentagrophytes was	(Kim, et al., 2008)

	T. mentagrophytes C. albicans	1-4 μg/mL MIC of C. albicans was 2-4 μg/mL	
3-18 nm AgNPs coated on catheters	Fungi: C. albicans	Potentially inhibited the growth of fungi	(Roe, Karandikar, Bonn-Savage, Gibbins, & Roullet, 2008)
10 nm AgNPs	Virus: HBV	Inhibition of HBV RNA	(Lu, et al., 2008)
1-10 nm AgNPs	HIV-1	Inhibition of HIV-1 by attaching host cells	(Elechiguerra, et al., 2005)

Gold nanoparticles (AuNPs) are adapted to a wide range of applications due to their distinct physical and chemical properties. Green synthesized AuNPs were used to evaluate antibacterial properties with *S.aureus*, *E. coli*, and *B. substilis*, and these AuNPs can also serve as an antioxidant (Lee, Nagajyothi, Sreekanth, & Park, 2015). There are two explanations for the mechanisms of AuNPs antibacterial properties. One is reported by Hamouda et al. which proposes that the positive charge of the Au ion is the key factor for its antibacterial activity via electrostatic attractions between the negatively charged cell membrane of bacteria and positively charged AuNPs (Hamouda, et al., 2001). Another explanation proposes that AuNPs can break

bacterial cell walls by damaging the permeability of the cell wall, resulting in leakage of the cell contents and eventually causing cell death (Rai, Prabhune, & Perry, 2010). Rai et al. reported that one-pot synthesized cefaclor capped spherical AuNPs (22-52 nm) were evaluated against gram-positive bacteria *S. aureus* and gram-negative bacteria *E. coli* and the minimum inhibition concentrations (MIC) were 10 μg/mL and 100 μg/mL, respectively (Rai, Prabhune, & Perry, 2010). In another study, irregularly shape AuNPs were synthesized by *G. elongata* extract showing high antibacterial activity, where it was reported that for *E. coli* and *K. pneumoniae* the maximum inhibition zones are 13.5 mm and 13 mm, respectively (Abdel-Raouf, Al-Enazib, & Ibraheem, 2013).

2.2.2 Heavy metal detection

Heavy metals have been known as an important threat to the environment and human health. Heavy metals cannot be biodegraded, and they can accumulate inside the animal body. Due to the food chain systems, continued exposure to heavy metals can resulting in eventual accumulation inside the human body (Mingorancea, Valdés, & Oliva, 2007) (Dai, et al., 2012) (Johnson, Wallace, Cashman, Granados, & Kent, 2008). A continued human exposure to heavy metal may lead to various diseases. For example, lead can cause neurological and cardiovascular disease, and mercury can cause serious damage to the central nervous system of human brain (Kim, Ren, Kim, & Yoon, 2012) (Clarkson, Magos, & Myers, 2003) (Godwin, 2001). Therefore, an accurate heavy metal detection method is necessary for environmental samples. Noble metal based nano-sensors have the potential advantages of being cheap, and fast, with simple sample preparation (Lee, Han, & Mirkin, 2007) (Darbha, et al., 2008) (Li, Wieckowska, & Willner, 2008).

Silver and gold nanoparticle based colorimetric sensors are suited for many heavy metal ions. For example, triazole-carboxyl functionalized AgNPs were synthesized to detect Co^{2+} in aqueous solution (Yao, 2010). In this study, AgNPs aggregated via metal ligand interactions with a color changed from yellow to red when the Co^{2+} was present in solution, and the minimum effective concentration (MEC) of AgNPs was 10 μM (Yao, 2010). Furthermore, AgNPs coated by polydopamine were prepared by a one-pot method and used to determine Hg^{2+}, by polydopamine adsorption of Hg^{2+} which thereby caused aggregation of AgNPs (Luo, Wang, & Tan, 2012). Here, the minimum effective concentration for AgNPs detection of Hg^{2+} was 50 nmol/L (Luo, Wang, & Tan, 2012). Additionally, citrate-capped AgNPs associated with H_2O_2 could detect Hg^{2+} as lower as 2 nM, but without H_2O_2 the minimum effective concentration of this cit-AgNPs was only 10 μM (Wang, Zhu, Jiao, Dong, & Li, 2012). Also, when H_2O_2 was present in the solution the color change in seconds (Wang, Zhu, Jiao, Dong, & Li, 2012). In another study, a novel method of Hg^{2+} detection was based on Hg^{2+} inhibition of the aggregation of AgNPs. This inhibition was caused by adding 6-thiogyanine to AgNPs, after adding Hg^{2+} into the solution, and the color stopped changing from brown to yellow (Duan, Yin, Wei, & Wang, 2014). In many articles, gold nanoparticles were also widely used to detect heavy metals. A highly selective quaternary AuNPs modified by ammonium group-terminated thiols can determine Hg^{2+}, because Hg^{2+} reacted with thiols and caused the aggregation of AuNPs (Liu, et al., 2010). A colorimetric sensor for detention of Ni^{2+} was developed with histidine and nitrilotriacetic acid (NTA) modified AuNPs (Krpetic, 2012). CTAB stabilized AuNPs were used to determine Cu^{2+} in aqueous solution, where the mechanism of this reaction was based on Cu^{2+} etching AuNPs with the assistance of $S_2O_3^{2-}$, and the minimum effective concentration was 30 nM and the color

change could be visually observed (Chen, et al., 2013). Table 2.5 lists some typical examples of colorimetric assays based on aggregation of Ag/AuNPs.

Table 2.5 Typical example of colorimetric assay based on aggregation of Ag/AuNPs.

Nanoparticles	**Sensing strategy**	**Minimum effective concentration**	**Reference**
AgNPs	Bared AgNPs aggregated by adding Hg^{2+}, due to the mercury-specific oligonucleotides (MSO) change from random coil structure to hairpin structure.	17 nM	(Wang, Yang, & Yang, 2010)
AuNPs	Cr^{3+} induced AuNPs aggregation, color change from red to blue.	13.42 nM	(Shellaiah, Simon, Suna, & Ko, 2015)
AuNPs	Glutathione (GSH) functionalized AuNPs were induced by Ni^{2+}	-	(Fu, Li, & Yang, 2012)
AuNPs	Glutathione (GSH) functionalized AuNPs were induced by Pb^{2+}	-	(Chai, Wang, Wang, Li, & Su, 2010)

AuNPs	Pb^{2+} induced of triazole-acetate functionalized AuNPs	16.7 nM	(Lee I. S., 2014)
AuNPs	DNA funtionalized AuNPs detected of Hg^{2+}	60 nM	(Wu, et al., 2011)
AuNRs	The deprotonated amine group of L-arginine on the AuNRs bound with Hg^{2+} leading to the side-by-side assembly of AuNRs	5 nM	(Guan, Wang, & Gunasekaran, 2015)

2.3 Summary

AgNPs have been synthesized by many ways, and there are many opportunities to control the shape of AgNPs. Different shaped AgNPs could provide different useful properties and uses in various areas. For example, triangular AgNPs have strong SPR properties, which could be used for colorimetric assays and surface-enhanced Raman spectroscopy studies. In addition, the special properties of AgNPs for antibacterial activity could be explored for many products. Furthermore, attaching AgNPs to biopolymers may provide an enhanced antimicrobial effect, and additional research on alternative biopolymers is a useful path.

Based on the intensity colors and strong SPR, Ag/AuNPs have been used in heavy metal ions detection for a long time. There are opportunities to explore additional heavy metals sensing

mechanisms. Additionally, from the previous literatures, Ag-Au alloys have not been fully examined with respect to their potential application ad sensing devices.

Chapter 3

Triangular Silver Nanoparticles Coated with Poly-L-lysine for anti-bacterial purposes

3.1 Abstract

Silver nanoparticles (AgNPs) have been widely used as anti-bacterial and anti-fungal agents in recent years, however they are unstable at higher ionic strengths and even ambient light may cause nano-silver aggregation. This study is an attempt to enhance the anti-bacterial properties of AgNPs by conjugating with a cationic biopolymer, Poly-L-Lysine (PLL), which contains functional amine groups. It has been widely used as a cell adhesion agent. PLL is also a kind of food additive, and it can resist or affect Gram-negative bacteria. Thus, the combination of AgNPs and PLL could not only increase the stability of AgNPs, but also enhance their antimicrobial properties. Gram-negative bacteria *Escherichia coli* and *Pseudomonas aeroginosa*, and Gram-postive bacteria *Bacillus subtilis* and *Staphylococcus aureus* were used to study the anti-bacterial properties of AgNP-PLL nano-composites. The results of transmission electron microscopy (TEM), UV/Vis-spectroscopy, zeta-potential and dynamic light scattering (DLS) indicate that the AgNP-PLL have the property of broad-spectrum activity for both Gram-negative bacteria and Gram-positive bacteria. The bacteria test shows good results, such that when AgNP-PLL was applied to the bacterial strains *E. coli* decreased by 97.27 %, *P. aeroginosa* decreased by 99.2%, *B. subtilis* decreased by 99.14%, and *S. aureus* decreased by 94.6% in 4 hours.

3.2 Introduction

Microbial contaminants are one of the significant causes of human illness, and the World Health Organisation (WHO) reports that faeces from humans and animals are a major source of risks, through the ingestion of water that is contaminated by faeces, which can be a source of pathogenic bacteria, viruses, and parasites (World Health Organisation, 2011). In 2008, over two million people died because of diarrheal diseases caused by polluted water (World Health Organisation, 2011). Therefore, to ensure the quality of delivered domestic water, it is important to find new materials able to kill microbes.

Traditional anti-bacterial methods use antibiotics that are extracted from medicinal plants, like Gunnera perpensa, Harpephyllum caffrum, Hypoxis latifolia and Ledebouria ovatifolia, etc (Buwa & Staden, 2006) (Palombo & Semple, 2001). In addition, pharmaceutical antibiotics are also be widely used, such as aminoglycoside, penicillin, carbapenems, etc (Bax, 1997) (Davies & Wright, 1997) However, the problems with antibiotics are that one kind of antibiotic may only be active against one kind of bacteria. Most of these extracts from such plants are active against Gram-positive bacteria, and only a few plant extracts show activity against Gram-negative bacteria (Palombo & Semple, 2001). The frequent occurrences of antibiotics resistance in bacteria indicate that there is a need for studying new and effective treatments. The unique properties of some nano-materials make them a candidate for antibacterial applications.

Silver based antiseptics are related to broad-spectrum anti-bacterial activity and have a much lower propensity to cause bacterial resistance than antibiotics. Silver ions (Ag^{+}) have been well known for their antibacterial and antifungal properties for a thousand years, and they have been widely used in dental work, wounds treatment, orthopaedic infections, catheters, fabrics, water purification, deodorants, and filters (Crabtree, et al., 2003) (Varner, El-Badawy, Feldhake, &

Venkatapathy, 2010). The effectiveness of silver ions has been demonstrated to be extended by release in a steady and prolonged manner from a silver-filled polyamide composite system (Kumar & Münstedt, 2005). The reason why silver ions (Ag^{+}) have been widely used is that they are highly toxic to microbes, but have low toxicity to mammals (Zhao & Stevens, 1998). In addition, scientists have found that silver nanoparticles (AgNPs) are able to seriously damage the structure of infectious microbes and are active against a broad-spectrum of Gram-positive and Gram-negative bacteria, including antibiotics resistant bacteria (Burrell, Heggers, Davis, & Wrigh, 1999) (Rai, Yadav, & Gade, 2009). Recently, the plasmonic properties of AgNPs have been used as an anti-bacterial and biosensor agent (Kim, et al., 2007). Additionally, developed nano-techniques enable scientists to synthesize AgNPs with various sizes, and manipulate the shape and surface properties of AgNPs. There are mainly two methods to synthesize AgNPs. The first is an irradiation method that can synthesize AgNPs with a chiseled shape and size via laser irradiation (Abid, Wark, Brevet, & Girault, 2002) (Eustis, et al., 2005) and microwave irradiation (Chena, Wang, Zhang, & Jin, 2008). The second method uses chemistry with sodium borohydride as the typical reducing agent (Lee & Meisel, 1982) (Shirtcliffe, Nickel, & Schneider, 1999).

However, one of the challenges is that AgNPs is that they are unstable in aqueous solution (Mafune, Kohno, Takeda, & Kondow, 2000) (Solomon, Bahadory, Jeyarajasingam, Rutkowsky, & Boritz, 2007). In this study, the biopolymer Poly-L-lysine (PLL) was used as a carrier of the AgNPs, to increase the stability of the AgNPs and to enhance the anti-bacterial ability (Kelly, Keegan, & Brennan-Fournet, 2012). Since PLL is a strong cell-adhesive agent and has a branched structure, it was hypothesized that it could connect with and increase the utilization of AgNPs by delivering them more efficiently to the cell surface. PLL is a metabolic product

produced by *Streptomyces* bacterial strains via a process of extraction, purification and separation (Krikorian, et al., 2002).

The chemical food additives allowed in the international market contain ascorbic acid, benzoic acid, propionate, acetic acid and their salts (Health Canada, 2013), among others. However, safety issues limit those additives capability. Thus, it is important to research effective, nontoxic, broad-spectrum natural food additives. PLL is a new type of natural food additives composed of L- lysine, an essential amino acid for the human body; it can be digested by the human body and become a human nutrition supplement. The unique property of PLL makes it a potential food additive, and also it can also produce anti-bacterial properties in neutral solution. The general concept of polypeptides acting as a nano-composites matrix involves various kinds of feasibilities for the programming and synthesis of multifunctional materials (Krikorian, et al., 2002).

For this research, AgNPs and nano-composites of AgNPs-PLL were prepared, and the morphology was observed via transmission electron microscopy (TEM). Surface potential and particle size distribution of the AgNP-PLL were measured with zeta-potential and dynamic light scattering (DLS). Anti-bacterial properties of the AgNPs-PLL nano-composites were assessed with plate count bacterial tests using two Gram-negative (*E. coli* and *P. aeruginosa*) and two Gram-positive (*B. subtilis* and *S. aureus).* The main structure difference between Gram-positive bacteria and Gram-negative bacteria cells is that Gram-positive bacteria have a thick peptidoglycan cell wall that contain lipoteichoic acid and is flexible, while the Gram-negative bacteria peptidoglycan layer is thinner and covered by plasma membrane (Beveridgr, 1999). The results of other researchers indicate that the AgNPs are antibiotic and can inhibit the formation of the peptidoglycans and lyse bacteria cell walls, thereby killing the bacteria (Fayaz, et al., 2010).

With the growth of antibiotics resistance and high-priced health product, silver-based reagents have the potential advantages of lower cost, broad-spectrum activity and high efficacy.

3.3 Materials and Methods

3.3.1 Reagents and Materials

Poly-L-lysine (PLL, 0.01 w/v%) solution was purchased from Sigma-Aldrich, with a number-average molecular weight of 70,000-150,000, sterile-filtered and suitable for cell culture. Silver nitrate ($AgNO_3 \geq 99\%$) was purchased from Sigma-Aldrich and stored in dark conditions. Sodium citrate ($Na_3C_6H_5O_7$, $\geq 99\%$) and hydrogen peroxide (H_2O_2, 30 wt%) were purchased from British Drug Houses (BDH), for use as a stabilizer and oxidizing agent, respectively. Sodium borohydride ($NaBH_4 \geq 98\%$) was purchased from Sigma-Aldrich, and used as a reducing agent. Polyvinylpyrrolidone (PVP), with a molecular weight of 40,000, was purchased from Sigma-Aldrich for use as a positive charge capping agent. Plate count agar and McConkey Agar were purchased from the HiMedia Company. Nutrient Broth Agar and Cetrimide Agar were purchased from Sigma-Aldrich. All the bacterial species in this study were purchased from Cedarlane Laboratories, Burlington, Ontario. The human cervical cancer (Hela) cell line was obtained from American Type Culture Collection, MD, USA.

3.3.2 AgNPs-PLL Nano-composites

The method for the synthesis of AgNPs colloid proposed by Shi and Sun (Shi & Ma, 2010) (Sun & Xia, 2002) was modified in order to achieve a 600 nm absorption wavelength as determined by UV/Vis-Spectroscopy. Under vigorous vortexing, 44.12 mg sodium citrate was added into 10 mL DI water, to which 0.1 mL $AgNO_3$ (30mM) and 0.17 mL H_2O_2 (30%) were

then added. After mixing well, 0.67 mL $NaBH_4$ (100mM) was injected rapidly, and vortexing continued until the color changed to dark green.

The AgNPs were left for 24 hours to stabilize, then the same volume of PLL (0.01%) solution was added to synthesis the AgNPs-PLL nano-composites. When the color changed to orange-yellow 5.47 mL PVP (0.2%) solution was added as a capping agent to stabilize the AgNPs-PLL nano-composites as a final product (Dong, Ha, Binh, & Kasbohm, 2012).

3.3.3 Bacteria Strains

The Gram-negative bacteria *Escherichia coli (ATCC PTA-4752) and Pseudomonas aeroginosa (ATCC 15442),* and the Gram-positive bacteria *Bacillus subtilis (ATCC 6051)* and *Staphylococcus aureus (ATCC 6538)* were chosen to test the anti-bacterial properties of the AgNP-PLL.

1) Agar plates and nutrient broth preparation Plate count agar 11.75g was suspended in 1000 mL DI water, and heated to boiling to dissolve the medium completely. Nutrient broth 5g was dissolved in 250 mL deionized water. Both were then sterilized by autoclaving at 15 lbs pressure (121°C) for 20 minutes. After autoclaving, hot Agar solution was poured into sterile Petri plates in a sterile environment.

2) Bacterial cultures Bacteria were cultured in flasks with 50 mL Nutrient Broth Agar at 37°C for 24 hours. To prepare the diluted bacterial solution, 1 mL of the culture was pipetted from the cultured flask into a 1.5 mL microcentrifuge tube. After washing twice with DI water the pellet was moved into a 50 mL centrifuge tube and filled with DI water to 40 mL. Then a serial dilution method was used to prepare 3 dilutions from this solution (100 times, and 1000 times dilutions).

3) Antibacterial solution preparation AgNP-PLL nano- composite, AgNPs and PLL solutions were used for antibacterial tests. 1mL of those samples were added to 9mL of above-mentioned bacteria strains solution. The solution was placed onto an incubator shaker at 120 rpm and maintained at 37°C for 4 hours. The control sample was prepared in the same protocol, but AgNP-PLL was replaced with DI water.

After incubation, took 50μL of the bacterial solution was added to the surface of a plate count agar in a sterile environment, and the solution was spread with a sterile spreader to homogeneously cover the surface. These four agar plates were placed in an incubator for colony growth at 37°C for 24 hours (Figure 3.7).

In this study, the AgNP-PLL nano-composite morphology was observed via transmission electron microscopy (TEM), using a Philips CM10 TEM. Surface potential and particle distribution of AgNP-PLL were measured with zeta-potential and dynamic light scattering (DLS), which were performed on a Malvern Zetasizer Nano-ZS90 instrument (Malvern, Worcestershire, UK). Inductively coupled plasma mass spectrometry (ICP) was performed by using a Prodigy High Dispersion ICP-OES. Absorbance of AgNP-PLL was observed using an HP 8542 Diode Array UV-visible spectrophotometer. Anti-bacterial properties of the AgNPs-PLL nano-composites were monitored with a plate count method. The results of bacterial reduction were calculated using the following equation:

$$R(\%) = \frac{N_b - N_s}{N_b}$$

where R is the reduction; N_b is the number bacterial colonies from an untreated sample, and N_s is the number bacterial colonies from the treated sample (Nelson, Marcato, Souza, Alves, & Esposito, 2007).

3.3.4 Hela Cells line

The cytotoxicity test procedure for AgNPs and AgNP-PLL activity used the typical method reported in the literature (Rai, Yadav, & Gade, 2009) (Wang & Liu, 2014). Hela cells (5,000 cells/ well) with 100 μm cell medium were dispensed into a 96-well U-bottom microplates, and incubated at 37°C in a humidified atmosphere of 5% CO_2 for 24 h. Then, the culture medium was replaced by 100 μm fresh prepared culture medium which contained AgNPs and AgNP-PLL with ten different concentration (18.6, 9.3, 4.65, 2.33, 1.16, 0.58, 0.29, 0.15, 0.07 and 0μg/mL and incubated for another 72 h.

The MTT assay was used to evaluate cell survival, where 25 μL methyl thiazolyl tetrazolium (MTT) solution (5 mg/mL in PBS) was added to each well to achieve a final concentration of 1 mg/mL. For the untreated sample, 25 μL MTT was replaced by 25 μL PBS. Then after incubation for 2 h, added 100 μL of extraction buffer (20% SDS in 50% DMF, pH 4.7, prepared at 37°C) was added into each well and incubation continued for 4 h. A SpectraMax M3 microplate reader was used to measure the absorbance at 570 nm.

3.4 Results and Discussion

3.4.1 Characterization of synthesized AgNPs

AgNPs were synthesized by the methods decribed in the Materials and Methods section, and the morphology was studied via TEM (Transmission electron microscopy) observation. To observe the in situ nanocomposite, samples were prepared on a carbon coated copper grid and dried at room temperature. Figure 3.1a shows a typical TEM micrograph of the AgNPs. An

approximately equilateral triangular morphology was observed with side length of 20-40 nm. Dynamic Light Scattering (DLS) results showed the size distribution of the AgNPs (Figure 3.2), with a peak value of 24.36 nm. This proves that the side length of most AgNPs are around 25 nm.

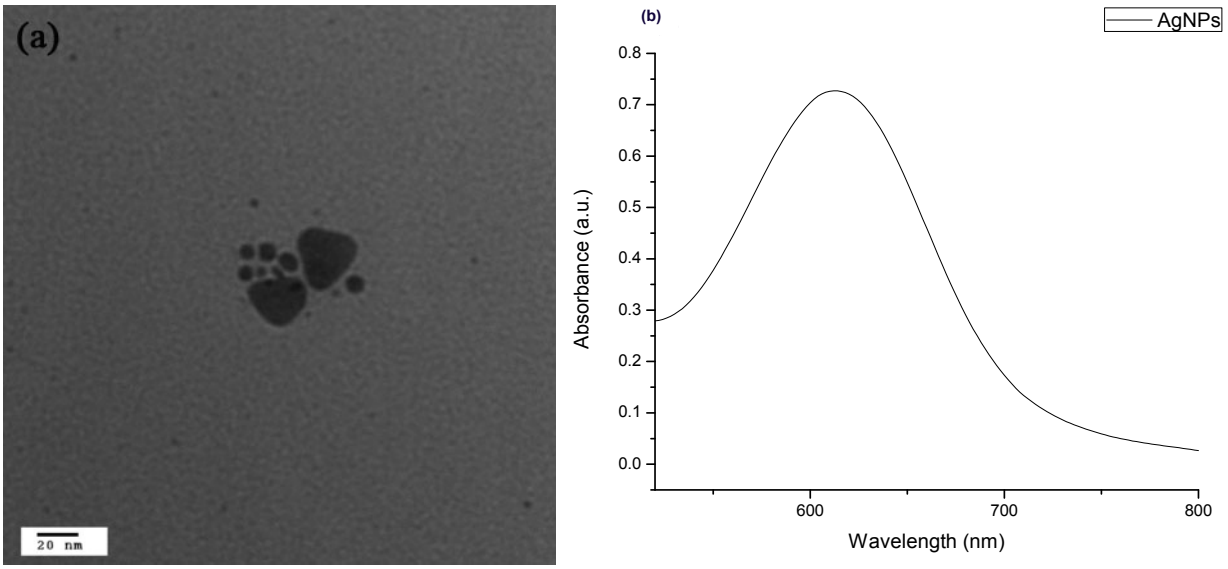

Figure 3.1 (a) TEM image of triangular silver nano particles at 20 nm scale bar. (b) UV/Vis-spectrum of silver nanoparticles.

The absorbance of AgNPs was measured via UV/Vis-Spectroscopy. The surface plasmon resonance of AgNPs is known to red-shift with a particle size increases, with the increased surface plasmon resonances resulting in a higher percentage of interaction than larger particles (Brause, Möltgen, & Kleinermanns, 2002) (Kerker, 1985) (Rai, Yadav, & Gade, 2009) (Pal, Tak, & Song, 2007) (Mulvaney, 1996). According to the research of Kelly, triangular AgNPs have a stronger surface plasmon resonance than spherical AgNPs, and based on the different size

of AgNPs the range of absorbance is 390-800 nm (Kelly, Keegan, & Brennan-Fournet, 2012). In the study of Guzman, the absorbance of 25 nm spherical AgNPs was maximum at approximately 418 nm (Guzman, Dille, & Godet, 2012). However, Figure 3.1b showns the results of this study, where the optical absorption spectrum of AgNPs peaked at 614 nm. This indicates that the edges of the trianglar AgNPs make the surface plasmon resonance shift to longer wavelengths.

The surface charges between AgNPs was studied using the Zeta-Potential Analyzer, and the result (-29.8 mV) demonstrated that the trianglar silver nanoparticles have negative electrostatic repulsion between them. Generally, a suspension that exhibits a zeta-potential less than - 20 mV is considered unstable and that may result aggregation in nanoparticles (Badawy, et al., 2010).

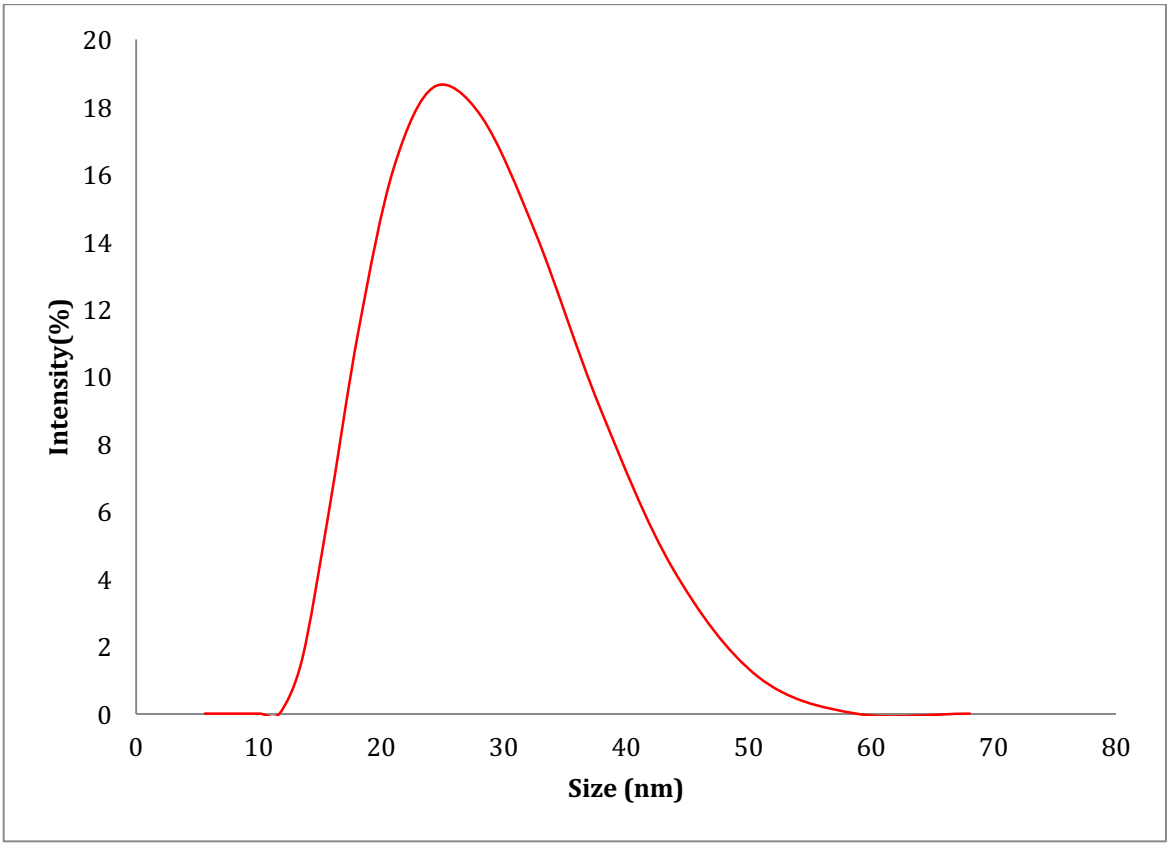

Figure 3.2 Size distribution of AgNPs as determined by dynamic light scattering (DLS).

3.4.2 Characterization of synthesized AgNP-PLL nano-composites

Stable AgNP-PLL nano-composites were obtained via the methods described in Section 3.3.2. In Figure 3.3, UV/Vis-spectroscopy showed that the absorbance peak of the AgNPs red-shifted from 614 to 650 nm and the optical density decreased from 0.73(a.u.) to 0.34(a.u.). The results indicate the surface plasmon resonance of silver nanoparticles decreased, which mean the color of AgNPs changed from green to yellow to form AgNP-PLL. Additionally, that demonstrates most AgNPs attached on the branches of Poly-L-lysine to become nano-composites structure. And the positive charges of the Poly-L-lysine neutralized the negative charges of silver nanoparticles. The zeta-potential of AgNP-PLL, as displayed in Figure 3.4 with a well-defined charge at 1.75 mV, illustrates that the positive charge of Poly-L-lysine neutralized the free ions of AgNPs.

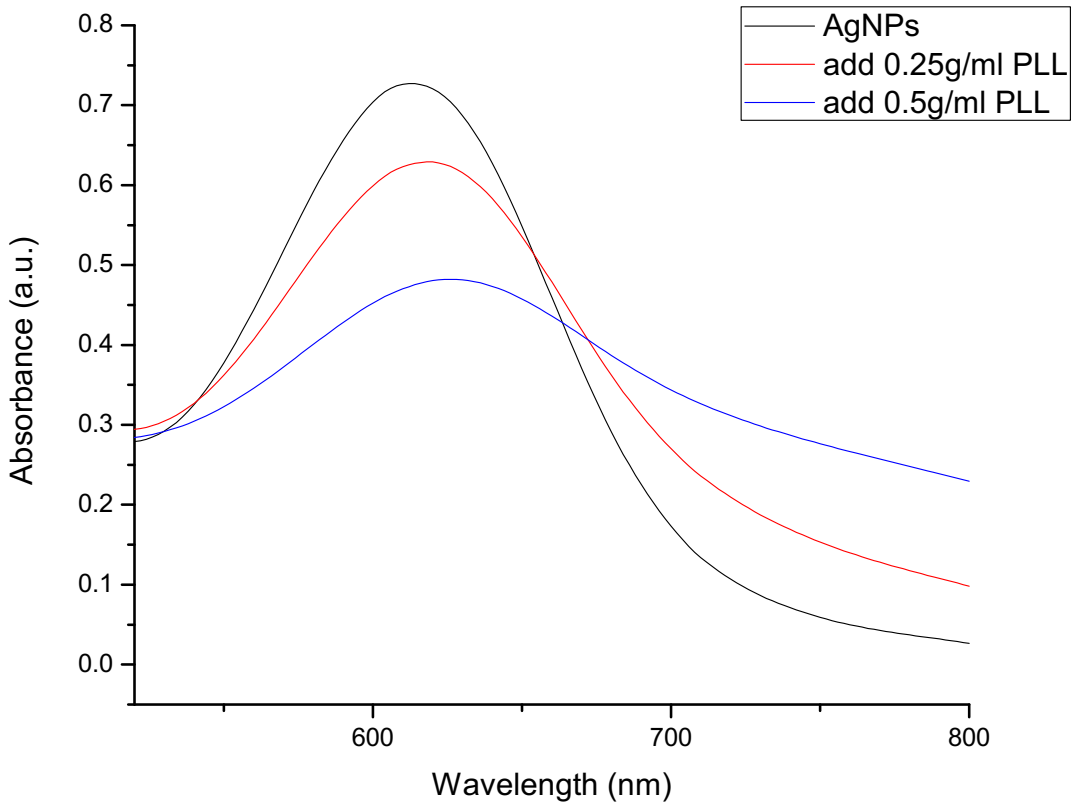

Figure 3.3 UV/Vis-Spectroscopy of AgNPs and silver AgNP-PLL.

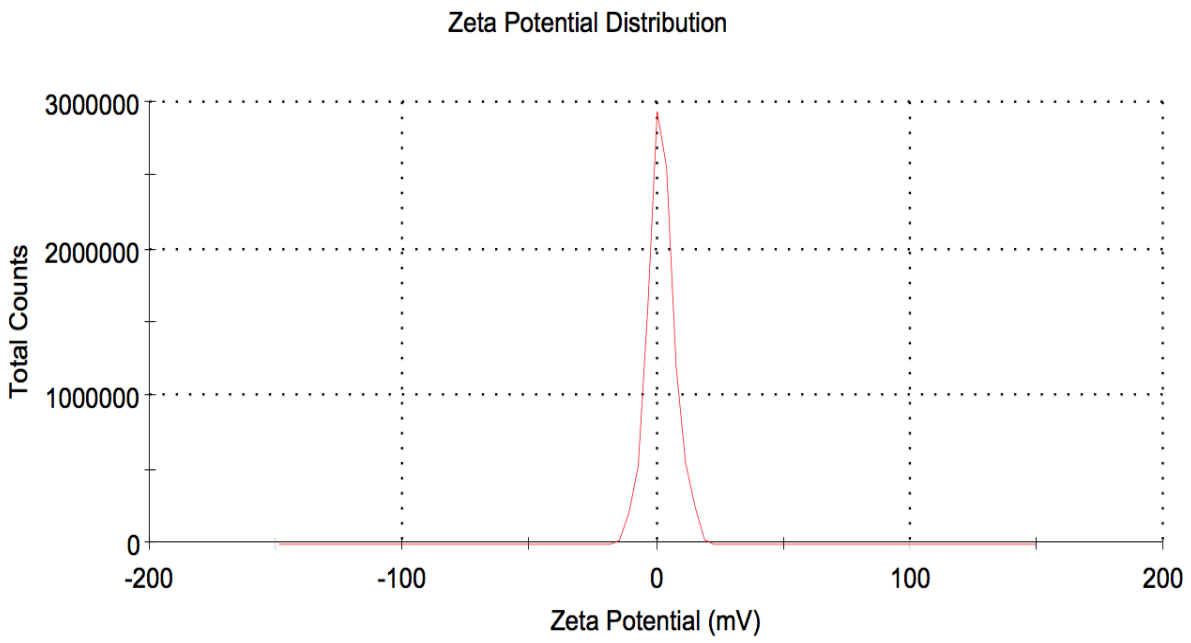

Figure 3.4 Zeta Potential of AgNP-PLL nano-composites

The observation using TEM, in Figure 3.5, shows that the sizes of the AgNP-PLL nano-composites are not uniform as the range is 50 nm-140 nm. And the PLL has lots of branches, which increase their body surface area. From the TEM image, it clearly shows silver nanoparticles are attached on the branches of the poly-L-lysine, and only a few of the free silver nanoparticles still can be seen in the solution. DLS results (Figure 3.6) show the size distribution of AgNP-PLL, with a maximum peak size centred at 122.4 nm.

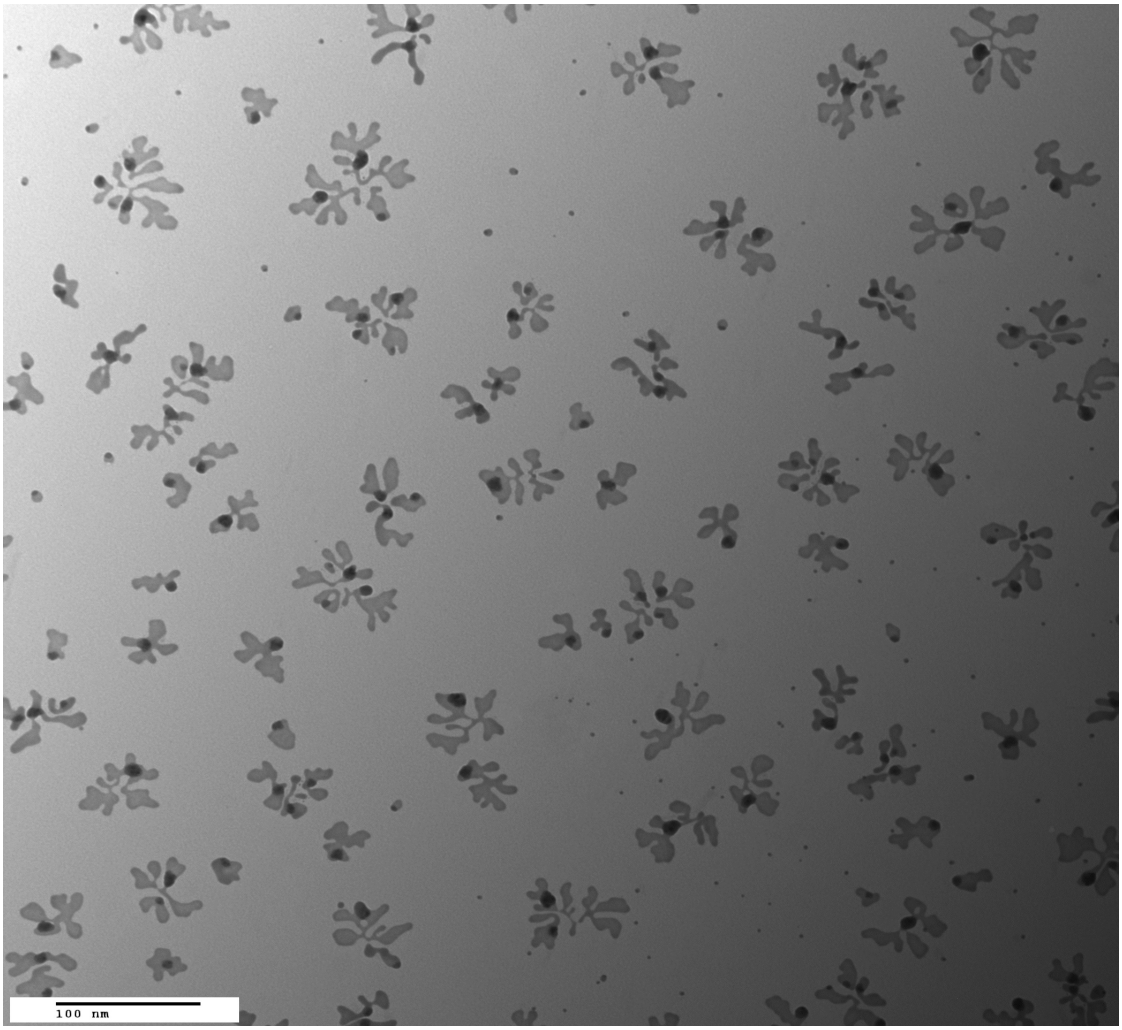

Figure 3.5 TEM image of AgNP-PLL nano-composites

According to the results of other researchers, PLL does not show branched structures when reacted with spherical AgNPs, and PLL was coated on the surface of spherical AgNPs to make to layer (Marsich, et al., 2012). The branches structure was showed in DNA binding studies, but the TEM images is not clearly as in this work (Li, et al., 2007). Therefore, in this reseach, the branched structure was first shown by reacting with trianglar AgNPs and make trianglar AgNPs adsorb on the branches. In addition, ICP-OES was used to determine the amounts of silver in

AgNP-PLL composites that is 18.6 µg/mL (302 moles of Ag/moles of PLL - 647 moles of Ag/ moles of PLL).

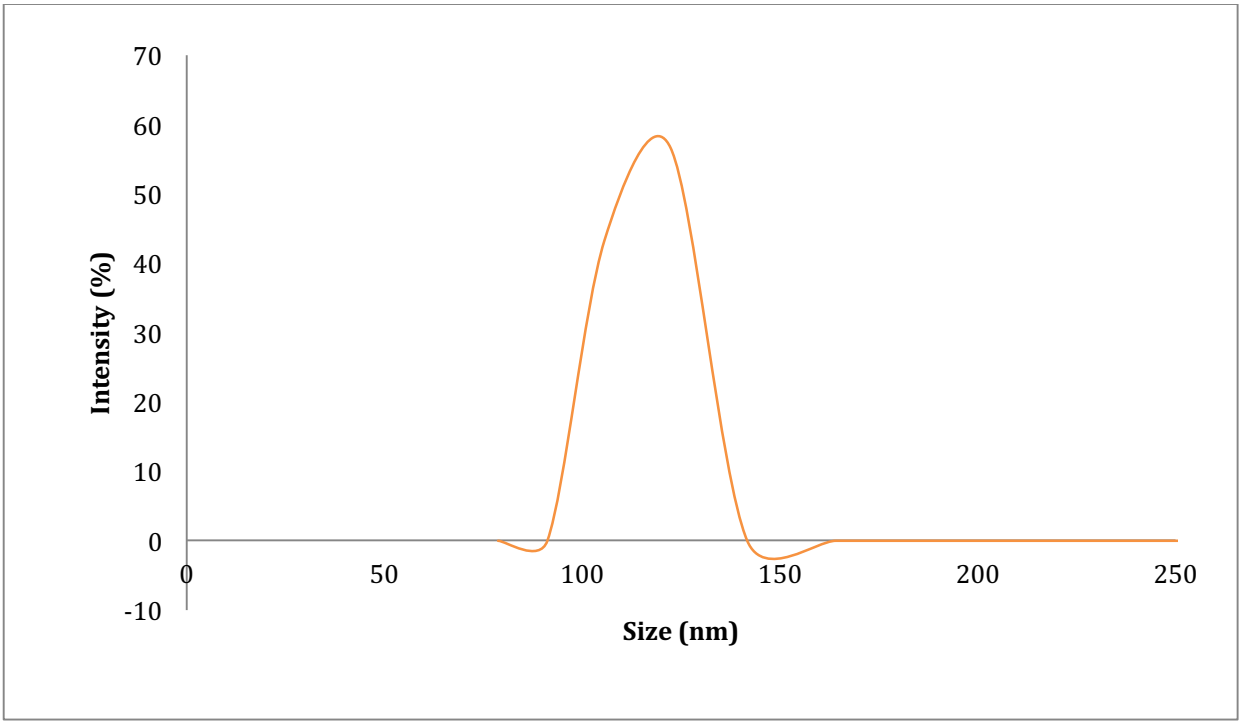

Figure 3.6 Dynamic Light Scattering AgNP-PLL size distribution by intensity.

3.4.3 Anti-bacterial test

The anti-bacterial activities of AgNPs-PLL nano-composites were measured via a plate count method. Gram-negative bacteria *E. coli* and *P. aeroginosa,* and gram-positive bacteria *S. aureus* and *B. subtilis* were chosen for this study.

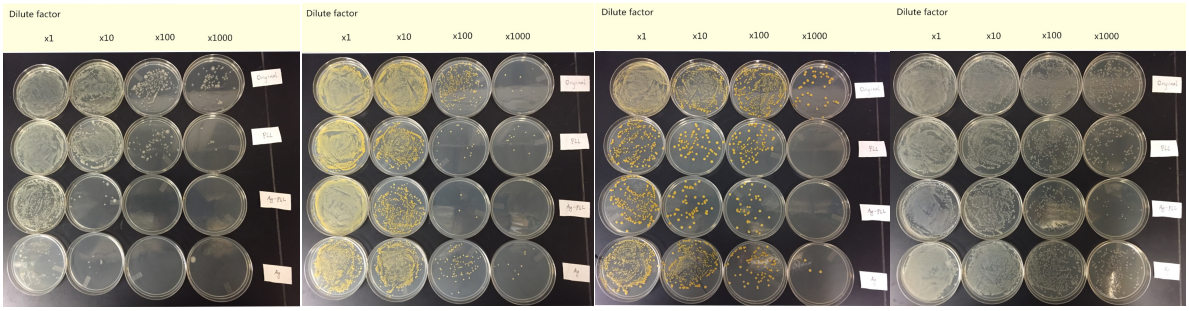

(a) (b) (c) (d)

Figure 3.7 (a) *E. coli* (b) *P. aeroginosa* (c) *S. aureus* (d) *B. subtilis*

Table 3.1 Plate count results of bacterial numbers in colony forming units/mL

	Gram-negative		Gram-positive	
	E. coli	*P. aeroginosa*	*S. aureus*	*B. subtilis*
	CFU/mL	CFU/mL	CFU/mL	CFU/mL
Control	33100	37300	27040	32000
PLL	9800	1800	380	6000
AgNP-PLL	904	300	232	1730
AgNPs	104	10200	2928	8120

The disposable plates were inoculated with the tested gram-positive and gram-negative bacteria, and the control sample of bacteria was at a concentration of about 104 cfu/mL. The comparison (Table 3.1) of AgNP-PLL, PLL, and AgNPs shows that: only for *E. coli*, the anti-bacterial activity of AgNP-PLL is not good as AgNPs, the bacterial reduction due to AgNPs is 99.7%, while the reduction by AgNP-PLL is 97.3%. For *P. aeroginosa, S. aureus*, and *B. subtilis*, the optimal anti-bacterial reagent is AgNP-PLL. The percentage reduction for *P. aeroginosa* is 99.2%, *S. aureus* is 99.1%, and *B. subtilis* is 94.6% (Figure 3.8). Researchers reported the reduction caused by AgBr/NPVP against *E. coli* and *B. cereus,* the minimum inhibitory concentration is 50μg/mL, which is two times higher than the concentration of AgNP-PLL in this study (18.6μg/mL) (Sambhy, MacBride, Peterson, & Sen, 2006). In a study in 2012, AgNP-PLL have an extra approximate 15% larger reduction than Ag/nepheline composite (85% against *E. coli* and 80% against *S. aureus*) (Ghafari-Nazari, Moztarzadeh, Rabiee, Rajablo, & Moza, 2012), and almost 99% anti-bacterial activity for AgNP-PLL for both gram-positive and gram-negative bacteria. Thus, the concentration of AgNP-PLL have almost 99% antibacterial activity is 1.86 μg/mL (calculated by ICP-OES results). Compared this results with a study of PD-CNC functionalized AgNPs in 2014, their concentration of AgNPs for 99% against *E. coli* and *B. subtilis* is 4μg/mL and 8μg/mL, respectively (Shi, et al., 2015).

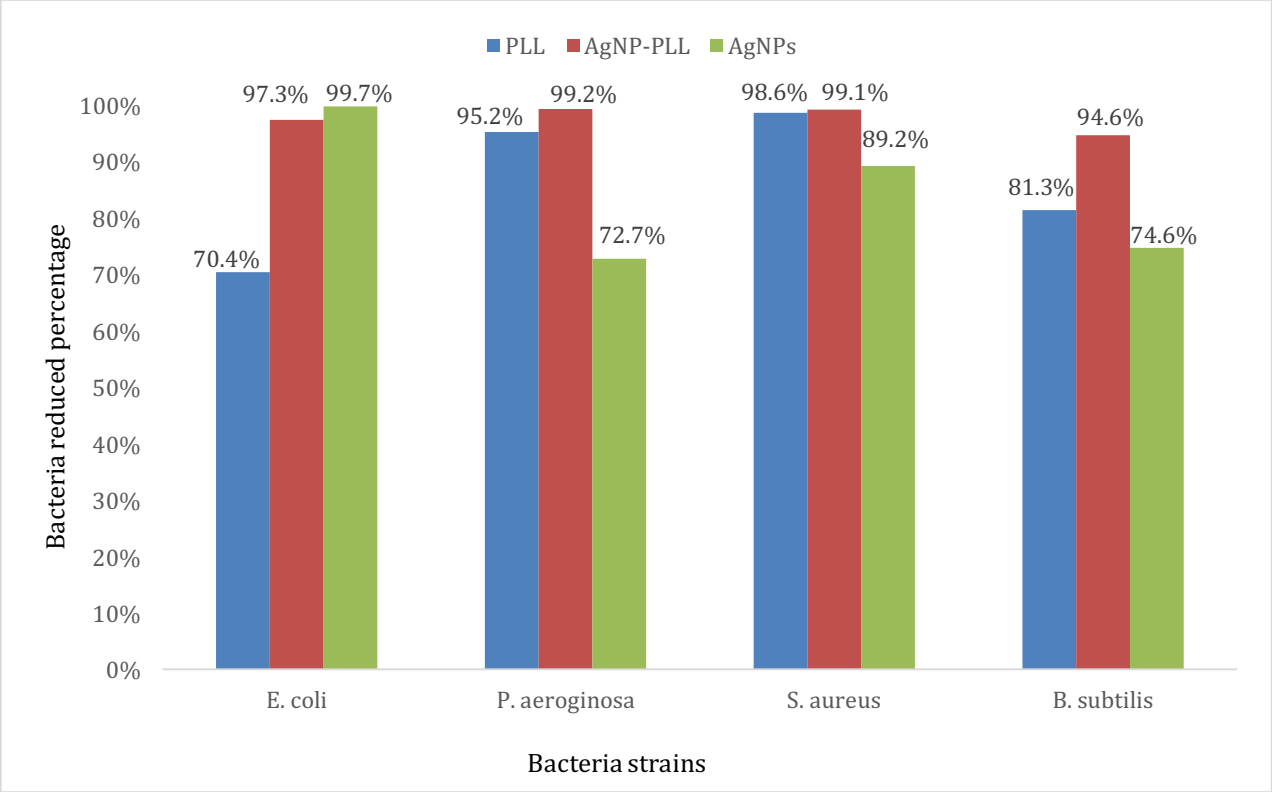

Figure 3.8 The optimal results of plates count for bacterial colonies reduced percentage.

The binding mechanism of AgNP-PLL with gram-positive and gram-negative bacteria was studied by TEM. Figure 3.9 shows that AgNP-PLL attached on the surface of bacterial cells and likely interfered with the cell's membrane permeability and respiration (Murray, Steed, & Elson, 1965). This phenomenon is hypothesized because the surface membrane of bacteria consists of lipopolysaccharides containing phosphate and pyrophosphate groups that make the bacteria surface negatively charged (Prescott, Harley, & Klein, 2002). Because of the AgNP-PLL weak positive charge and its branches increasing the surface area, it is reasonable to state that the binding of the nano-composites to the bacteria depends on the interaction of the available surface area. From the TEM images (Figure 3.9a), it is clearly shown that some AgNPs were able to

penetrate the bacterial cell and lead to likely further damage. It has been reported that AgNPs can affect bacterial DNA by reacting with phosphorus-groups (Gibbins & Warner, 2005). Also, the mechanism of reaction of silver is reportedly related to its interruption of the thiol-group compounds in the enzymes of bacterial cells, thus inhibiting the respiration process (Klasen, 2000) (Rai, Yadav, & Gade, 2009).

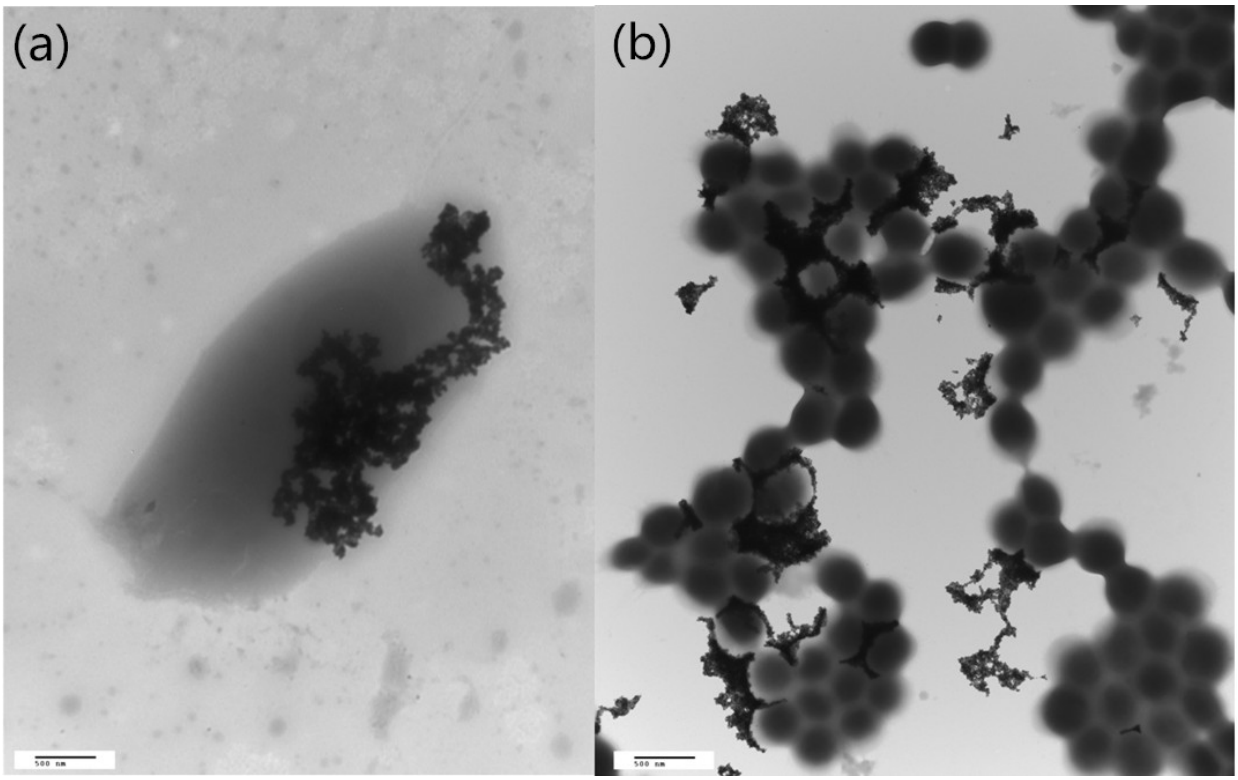

Figure 3.9 TEM images (a) AgNP-PLL nano-composites with Gram-negative bacteria *P. aeroginosa*. with 500 nm scale bar. (b) AgNP-PLL nano-composites with Gram-positive *bacteria S. aureus*. with 500 nm scale bar.

According to the results, AgNP-PLL nano-composites have a larger antimicrobial effect on Gram-negative bacteria strains than Gram-positive bacteria. This is likely due to the cell wall composition difference between Gram-positive and Gram-negative bacteria. Gram-positive bacteria have a thick peptidoglycan cell wall that contain lipoteichoic acid, while Gram-negative bacteria peptidoglycan is thinner and covered by a plasma membrane (Beveridgr, 1999) (Lin, et al., 2015). This plasma membrane is inflexible and easier to break than a peptidoglycan layer (Beveridgr, 1999). The plasma membrane has more negative charges that can attract the weak positive charge on the surface of AgNP-PLL. On the other hand, Gram-positive bacterial peptidoglycan layers contain linear polysaccharide chains that cross-link via short peptides and form a 3-dimensional strong structure. All these considerations provide evidence that the anti-bacterial activity of AgNP-PLL nano-composites against gram-negative bacteria is better than against gram-positive bacteria. But in either case, the effectiveness of biocidal action is nearly 100% for both gram-positive and gram-negative bacteria at the conditions used in this work.

3.4.4 Cytotoxicity Evaluation

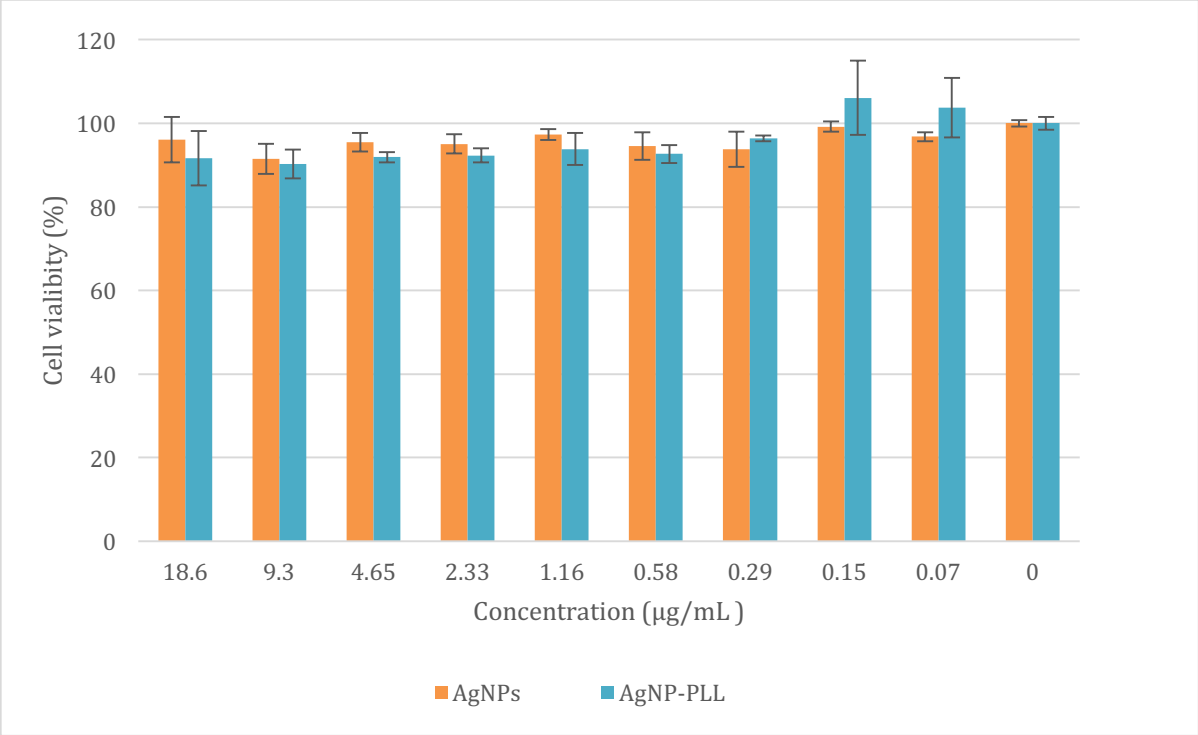

Figure 3.10 Viability of Hela cells measured via MTT assay in the presence of different concentration of triangular AgNPs and AgNP-PLL nano-composites after 72 h incubation.

The cytotoxicity effects of AgNPs and AgNP-PLL on Hela cells were tested and compared with the MTT assay. In Figure 3.10, the results of the present study showed that at higher concentrations ranging from 0.58 to 18.6 µg/mL, AgNPs have a lower toxicity effect on Hela cells than the AgNP-PLL nano-composites. When the concentration was lower than 0.58 µg/mL, both AgNPs and AgNP-PLL showed no significant toxicity to Hela cells. However, from the results, even the highest concentration (18.6 µg/mL) caused less then 10% cell death, which indicates that both AgNPs and AgNP-PLL are almost no toxicity to Hela cells.

3.5 Summary and Conclusions

A method that attached silver nanoparticles on the branches of Poly-L-lysine resulted in a new type of anti-bacterial nanomaterial. The results of TEM and DLS prove that the AgNP-PLL is around 120 nm and it has a branched structure which can increase the surface area available for interactions. UV/Vis-spectroscopy indicates the color change of AgNPs react with PLL, and zeta-potential reasonably demonstrated that AgNP-PLL has positive charges (+1.75 mV) that can be attracted to the negatively charged bacterial cell walls. Anti-bacteria test indicated AgNP-PLL has a strong antimicrobial ability against both gram-positive and gram-negative bacteria, with reductions as high as 99%, while remaining relatively nontoxic to Hela cells. In conclusion, this study indicates that the AgNP-PLL nano-composites have broad-spectrum activity and can be potentially used as low-cost and high efficiency anti-bacterial materials in such applications as wound treatment, dental work, orthopaedic infections, catheters, fabrics, water purification, deodorants, and filters.

Chapter 4

Triangular silver nanoparticles for rapid colorimetric detection of Hg^{2+} ions in aqueous solutions

4.1 Abstract

Toxic heavy metals have been considered to be one of the contaminants of concern in certain aqueous solutions. In this study, PVP stabilized triangular AgNPs were developed for the detection of mercury (II) (Hg^{2+}). AgNPs were characterized via TEM, DLS, and UV-Vis spectrophotometer, proving that the shape of the AgNPs are triangular with an intense surface plasmon resonance, and the zeta potential results indicate that the negative surface charge of the AgNPs (-27.6 mV) can attract Hg^{2+}. In a selectivity study, four kinds of heavy metals ions (Cr^{3+}, Pb^{2+}, Cd^{2+}, and Hg^{2+}) were applied in DI water. It was shown by TEM and UV-Vis spectrophotometry that the AgNPs were specific for Hg^{2+}, which acted as a bridge to induce AgNPs aggregation. The minimum effective concentration (MEC) that could be detected by the aggregation of these AgNPs was 0.938 μM, (188.2 ng Hg^{2+}/mL water). The optimal working pH range of the AgNPs for Hg^{2+} detection was pH 7 to 10. The reaction between AgNPs and mercury ions was established by inhibited assay with EDTA. From a study with tap water spiked with Hg^{2+} ions, AgNPs were slightly affected by ions in the tap water, but the sensitivity towards Hg^{2+} was exceptional (minimum effective concentration (MEC) is 1.25 μM).

4.2 Introduction

Heavy metal contamination has been known as one of the threats to the environment and public health. Once heavy metals are inside the body of an animal, they cannot be metabolized and they will accumulate inside body. Because of the food chain systems, those heavy metals could eventually accumulate or bio-magnify inside the human body (Mingorancea, Valdés, & Oliva, 2007) (Dai, et al., 2012) (Johnson, Wallace, Cashman, Granados, & Kent, 2008). Since heavy metals are non-degradable and persistent in ecosystems, they are highly toxic and can affect both plants and animals (Clarkson, Magos, & Myers, 2003) (Sharma, Katnoria, & Nagpal, 2016) (Ojekunle, et al., 2016). Human exposure to heavy metals could lead to various diseases, like irritability, anemia, muscle paralysis and memory loss, and those symptoms can cause harmful damage especially for children (Kim, Ren, Kim, & Yoon, 2012) (Clarkson, Magos, & Myers, 2003) (Godwin, 2001). Among heavy metals, mercury ion (Hg^{2+}) is considered as one of the most toxic heavy metal contaminants, since it can cause serious damage to the human brain and central nervous system (Langford & Ferner, 1999) (Carvalho, Chew, Hashemy, Lu, & Holmgren, 2008) (Clarkson, Magos, & Myers, 2003). Since mercury ion (Hg^{2+}) can be widespread in air, soil, and water (Kim, Ren, Kim, & Yoon, 2012), accurate methods for detection of Hg^{2+} are necessary.

Traditional techniques for analysis of Hg^{2+} in aqueous solutions include flame atomic absorption spectroscopy (FAAS) and atomic absorption spectroscopy (AAS), cold vapor atomic fluorescence spectrometry, inductively coupled plasma atomic/optical emission/mass spectrometry(ICP-AES/OES/MS) (Djedjibegovic, Larssen, Skrbo, Marjanović, & Sober, 2012) (Faraji, et al., 2010) (Moor, Lymberopoulou, & Dietrich, 2001), and high performance liquid chromatography (HPLC) (Nolan & Lippard, 2008). However, those techniques either require

expensive and complex equipment, or have complicated sample preparation procedures and long test times. Hence, a simple, efficient, and inexpensive method is desirable for detecting Hg^{2+} in aquatic and similar solutions.

In the past decade, nanotechnology has shown advantages in various areas of analysis. Since the size of nanoparticles is smaller than other materials, nanoparticles have a relatively large surface area (Riu, Maroto, & Rius, 2006) (Huang & Choi, 2007). Noble metal based nano-sensors have been developed to avoid complicated instrumentation and sample preparation (Lee, Han, & Mirkin, 2007) (Darbha, et al., 2008) (Li, Wieckowska, & Willner, 2008). Additionally, the correlation between special surface plasmon resonance shift of noble metal and the particle size change can be used as colorimetric sensor for heavy metal ions detection (Kelly, Keegan, & Brennan-Fournet, 2012).

In this study, AgNPs were chosen as a colorimetric probe. With the developing of chemical methods, silver nanoparticles have been synthesized with triangular shape, which increased the surface plasmon resonance of AgNPs (Shi & Ma, 2010) (Sun & Xia, 2002). Due to the correlation between the particular surface plasmon resonance peak and the particle size, AgNPs are used as colorimetric sensor of Hg^{2+} (Kelly, Keegan, & Brennan-Fournet, 2012). However, for effective and sensitive colorimetric detection of Hg^{2+}, it is necessary to synthesize AgNPs with appropriate surface ligands, which could specifically and efficiently interact with Hg^{2+}, and also that could stabilize the AgNPs, as it mentioned in Chapter 3 AgNPs are easily aggregated because their negative surface charge (Mafune, Kohno, Takeda, & Kondow, 2000) (Fan, Liu, Wang, & Zhan, 2009) (Badawy, et al., 2010) (Solomon, Bahadory, Jeyarajasingam, Rutkowsky, & Boritz, 2007).

4.3 Materials and Methods

4.3.1 Reagents and Materials

Potassium chromate (CrK_2O_4, ACS reagent, ≥99.0%), lead (II) nitrate (PbN_2O_6, ACS reagent, ≥99.0%), mercury (II) chloride ($HgCl_2$, ACS reagent, ≥99.5%), and cadmium chloride ($CdCl_2$, 99.99% trace metal basis) were purchased from Sigma-Aldrich, and used in the heavy metal selectivity assay. Ethylene diamine tetra acetic acid (EDTA) disodium salt dehydrate was purchased from Anachemia, and used for the interference study. Silver nitrate ($AgNO_3$, ≥ 99%) and sodium borohydride ($NaBH_4$, ≥ 98%) were purchased from Sigma-Aldrich. Sodium citrate ($Na_3C_6H_5O_7$, ≥ 99%) and hydrogen peroxide (H_2O_2, 30 wt%) were purchased from British Drug Houses (BDH). Buffer solutions from pH 5 to 10 were prepared with sodium phosphate monobasic dihydrate (BioUltra, for molecular biology, ≥99.0%) and sodium phosphate dibasic dihydrate (BioUltra, for molecular biology, ≥99.0%), which were purchased from Sigma-Aldrich. Polyvinylpyrrolidone (PVP), with a molecular weight of 40,000, was purchased from Sigma-Aldrich for use as a stabilizer. All the chemicals in this research were used as received.

4.3.2 Synthesis of Triangular Silver Nanoparticles

AgNPs were synthesized with a similar method described in Chapter 3.3.2, where 150 mg of sodium citrate was dispersed into 100 mL DI water, followed by adding 340 μm $AgNO_3$ (30 mM) and 560 μL H_2O_2 (30%). Then 2.3 mL $NaBH_4$ (100 mM) was injected rapidly, and kept shaking overnight. After that, PVP was added at the final concentration of 0.03%. The synthesized AgNPs were stored in the dark and used as a stock solution.

4.3.3 Heavy Metal Salts Stock Solutions

In this study, four environmentally toxic heavy metal ions were chosen, Cr^{3+}, Pb^{2+}, Cd^{2+}, and Hg^{2+}, and dissolved in DI water and laboratory tap water to a 10 μM concentration from their salts respectively. Then, mercury salt was further diluted with DI water for form concentrations of 5 μM, 2.5 μM, and 1.25 μM. EDTA was dissolved in DI water for inhibition studies. Six different pH values (pH 5.8, pH 6.5, pH 7.27, pH 7.8, pH 9.79) of phosphate buffer solutions were prepared at 10 μM.

4.3.4 Heavy metal salts preparation for AgNPs selectivity test

To determine if the AgNPs are specific for Hg^{2+} detection, three kinds of environmentally toxic metal cations (Cr^{3+}, Pb^{2+}, Cd^{2+}) were tested with AgNPs in aqueous solution to find out the sensing ability of AgNPs. Therefore Cr^{3+}, Pb^{2+}, Cd^{2+}, and Hg^{2+} were prepared in DI water at 10 μM to ensure there would be a sufficient colorimetric response. Phosphate buffer solution at pH 7.8 was used as method control and DI water was used as blank control.

4.3.5 Instruments

Transmission electron microscopy (TEM) characterization was performed using a Philips CM10 electron microscope. UV-visible spectroscopy was performed with a HP 8542 Diode Array UV-visible spectrophotometer. Surface potential and particle distribution of AgNPs were measured with zeta-potential and dynamic light scattering (DLS), which were performed on a Malvern Zetasizer Nano-ZS90 instrument (Malvern, Worcestershire, UK). Inductively coupled plasma mass spectrometry (ICP) was performed by using a Prodigy High Dispersion ICP-OES.

4.4 Results and Discussion

4.4.1 Characterization of AgNPs

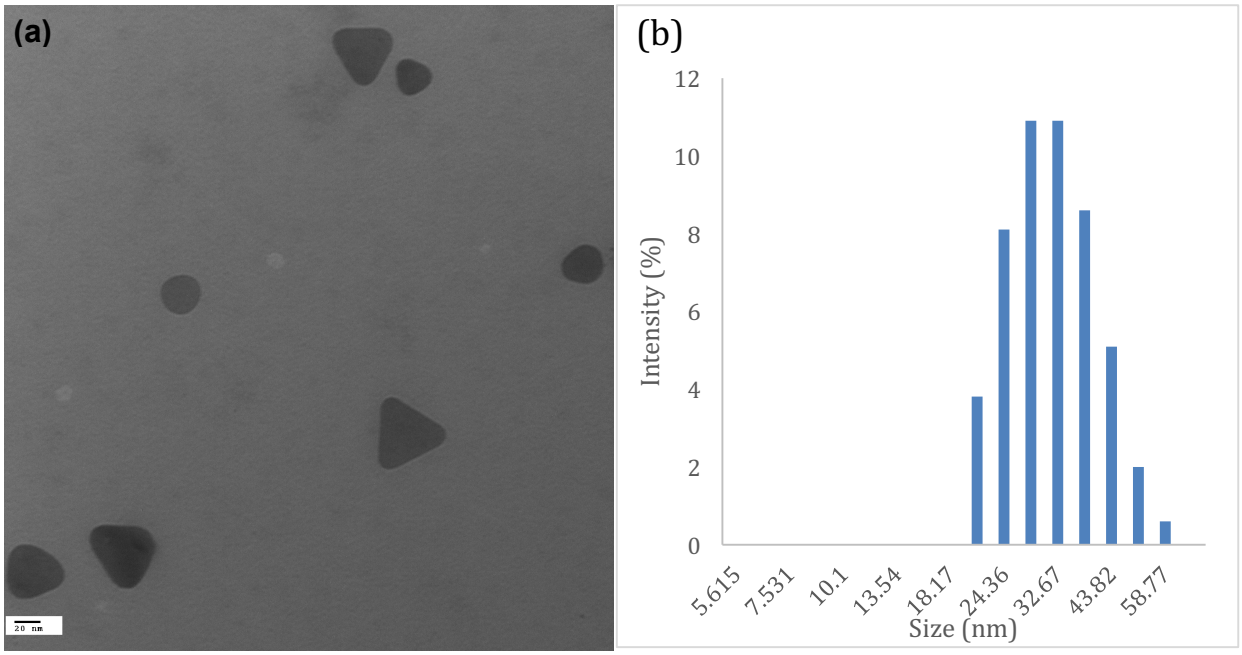

Figure 4.1 (a) TEM image of AgNPs at 20 nm scale bar. (b) Size distribution of AgNPs as determined by DLS.

The morphology and size distribution of the synthesized AgNPs were characterized by TEM and DLS as shown in Figure 4.1a and b, respectively, which indicates the properties of the separated triangular silver nanoparticles in the absence of Hg(II) ions. According to the TEM image (Figure 4.1a), the shape of most silver nanoparticles was triangular and the average particle size (the apex to the baseline) is around 35 nm ± 5 nm (Figure 4.1b), which is confirmed by particle size analyser DLS with a peak value of 34.5 nm. As mentioned in Chapter 3.4.1, these AgNPs have negative surface charges, which is confirmed in Figure 4.2, where the zeta potential analyzer shows that the AgNPs surface charge was -27.6 mV. However, when comparing these AgNPs with the AgNPs in chapter 3, these AgNPs are slightly bigger than the AgNPs in chapter

3. This is because, in this study, large volume reagents had been used, and this resulting in a slower the reaction rate than the synthesis described in chapter 3 (Pillai & Kamat, 2004).

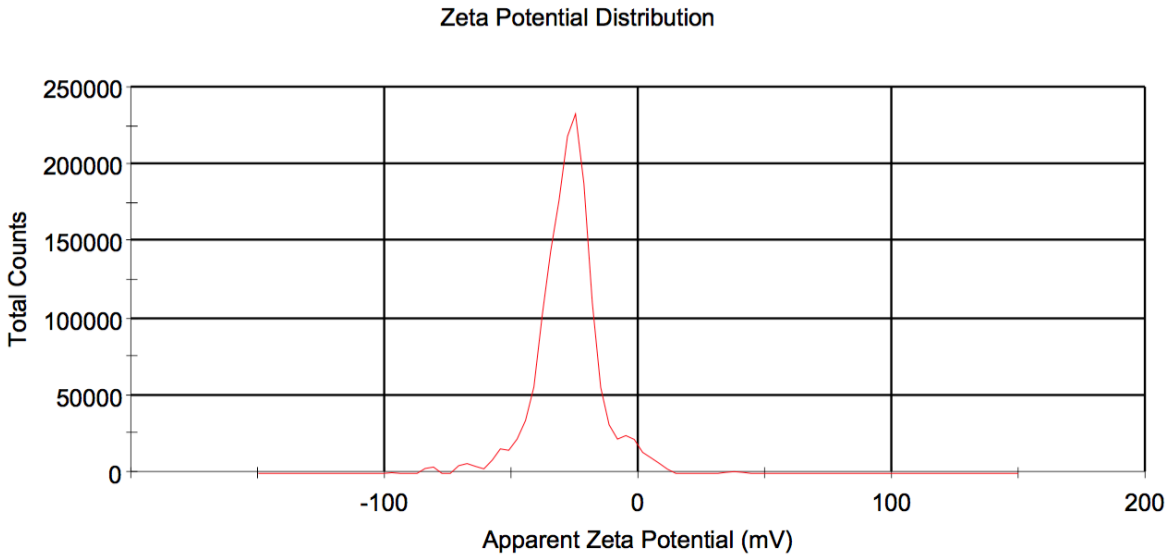

Figure 4.2 Zeta potential distribution of AgNPs

Because triangular AgNPs have a stronger surface plasmon resonance than spherical AgNPs (Kelly, Keegan, & Brennan-Fournet, 2012), and different particles size results in both different and a variety of colors, the absorbance of AgNPs as determined by UV-Vis spectrophotometer, with a peak absorbance at 660 nm as shown in Figure 4.3 was used in this study.

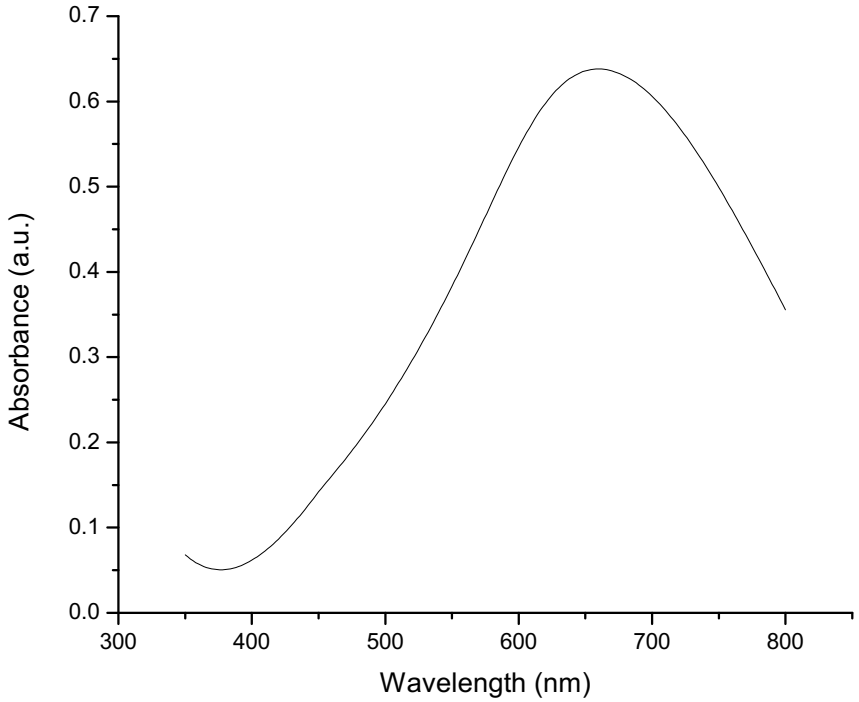

Figure 4.3 UV-Visible spectroscopy of AgNPs (18.6 μg Ag/mL).

4.4.2 Heavy Metal Ion Selectivity of AgNPs

In Figure 4.4, the effect of the heavy metal Hg^{2+} ions on the UV-Vis spectra absorbance of AgNPs in aqueous solution is demonstrated, by the very significant absorption peak shift of Hg^{2+} ions from 660 nm to 510 nm is very significant. This blue shift could also be observed by the naked eyes as a color change from blue to pink and eventually will change to yellow as shown in Figure 4.5. Thus, the results indicate that, except for Hg^{2+}, the rest of the heavy metal ions tested did not affect the absorption spectra and produce a color change in the AgNPs colloid, meaning that only the presence of Hg^{2+} causes this aggregation of AgNPs. The mechanism of this

phenomenal might because the redox reaction between Ag(0) and Hg^{2+} (Yuan, Wen, Shen, & Shi, 2013).

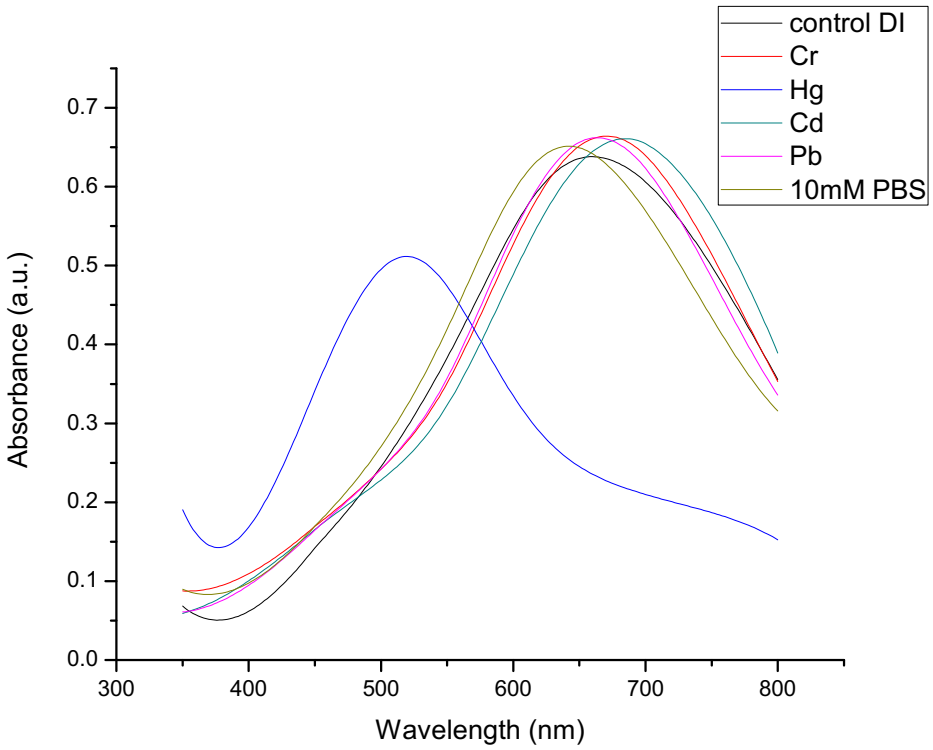

Figure 4.4 UV-Vis Spectroscopy of AgNPs in the presence of Cr^{3+}, Pb^{2+}, Cd^{2+}, and Hg^{2+} (10 μM).

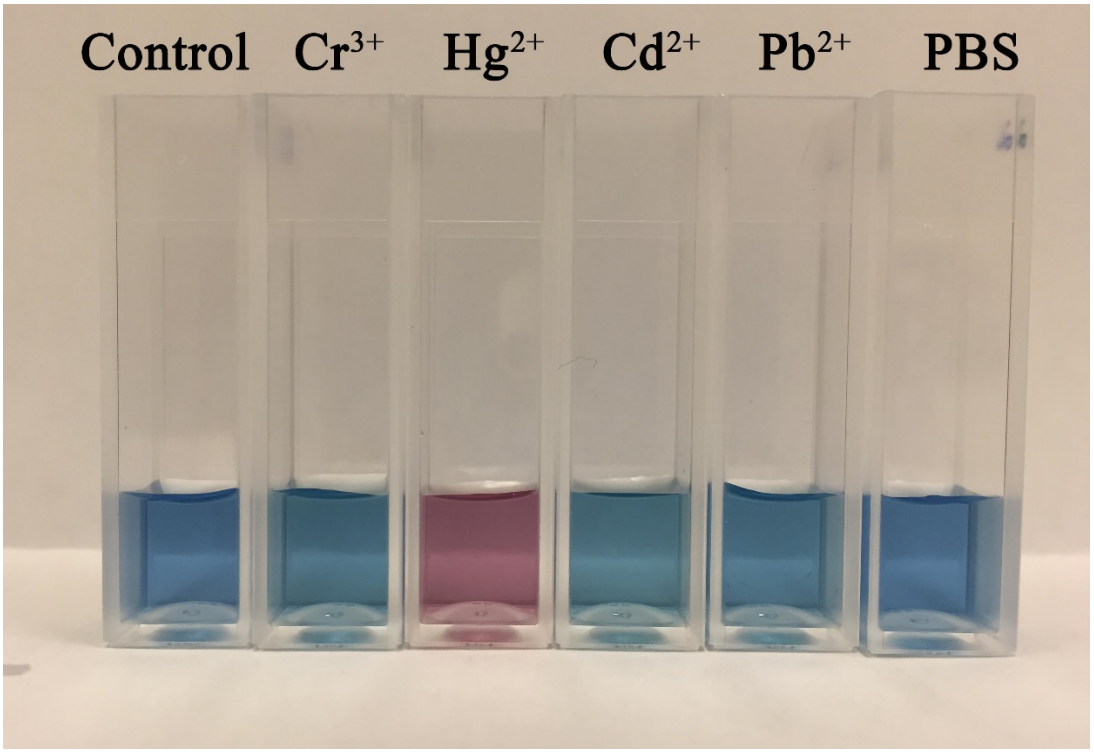

Figure 4.5 Photograph of sensor selectivity of AgNPs towards 10 μM of four kinds of heavy metal ions.

To confirm the selectivity results, TEM and DLS were used to characterize the AgNPs-Hg^{2+} mixture The TEM image (Figure 4.6a) clearly shows Hg^{2+} caused the aggregation of AgNPs. In contrast to the original size of the AgNPs (34.5 nm), the size of the aggregated AgNPs-Hg^{2+} is approximately 105.7 nm as shown in Figure 4.6b. Therefore, this is evidence that the Hg^{2+} acted as a bridge between silver nanoparticles to prompt the aggregation as shown in the TEM image.

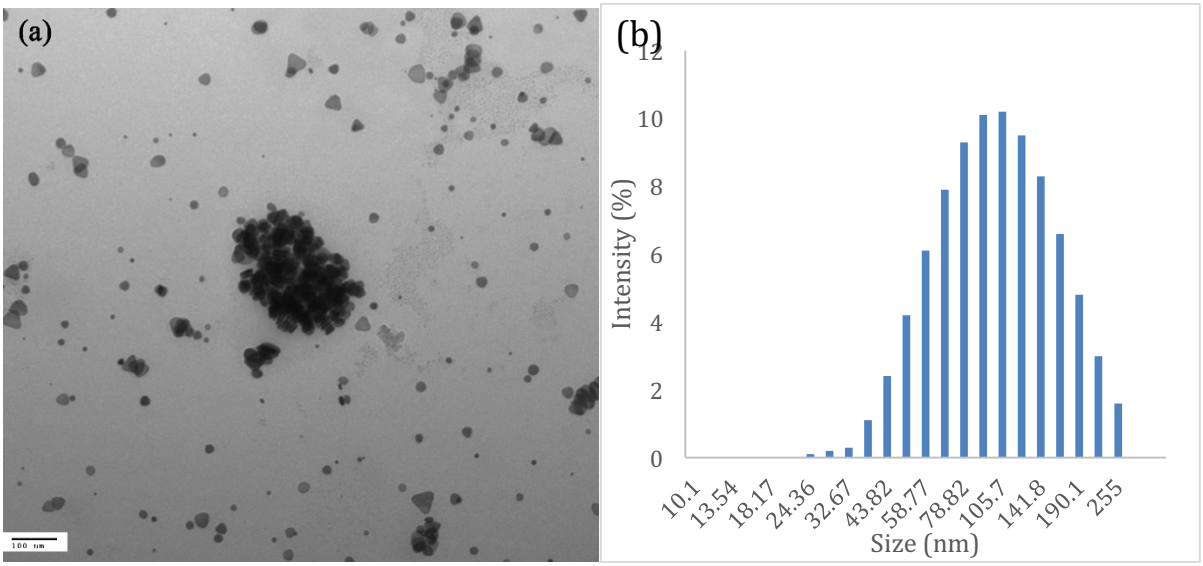

Figure 4.6 (a) TEM image of AgNPs-Hg^{2+} at 100 nm scale bar and (b) Size distribution of AgNPs-Hg^{2+} as determined by DLS.

To evaluate the aggregation degree of AgNPs, four concentrations of Hg^{2+} (10 μM, 5 μM, 2.5μM, 1.25μM) were measured. When Hg^{2+} was absent from the solution, the absorbance peak value of AgNPs is centred around 654 nm. When there is sufficient Hg^{2+} (like 10 μM) present in the solution, AgNPs will aggregate and the color will change from blue to yellow. With a shift of the absorbance peak of AgNPs from 654 nm toward 470 nm as shown in Figure 4.7a. Within a certain concentration range (0.938 μM-10 μM) of Hg^{2+}, there is a linear relationship between Hg^{2+} concentration and the AgNPs- Hg^{2+} absorbance peak wavelength (Figure 4.7b). With the continuing decrease of the Hg^{2+} concentration, a minimum effective concentration (MEC) will be found at the intersection point (Figure 4.6b) of the linear line and y=654 nm (the absorbance peak in the absence of Hg^{2+}). This MEC is 0.938 μM, which was calculated via the equation noted in Figure 4.6b.

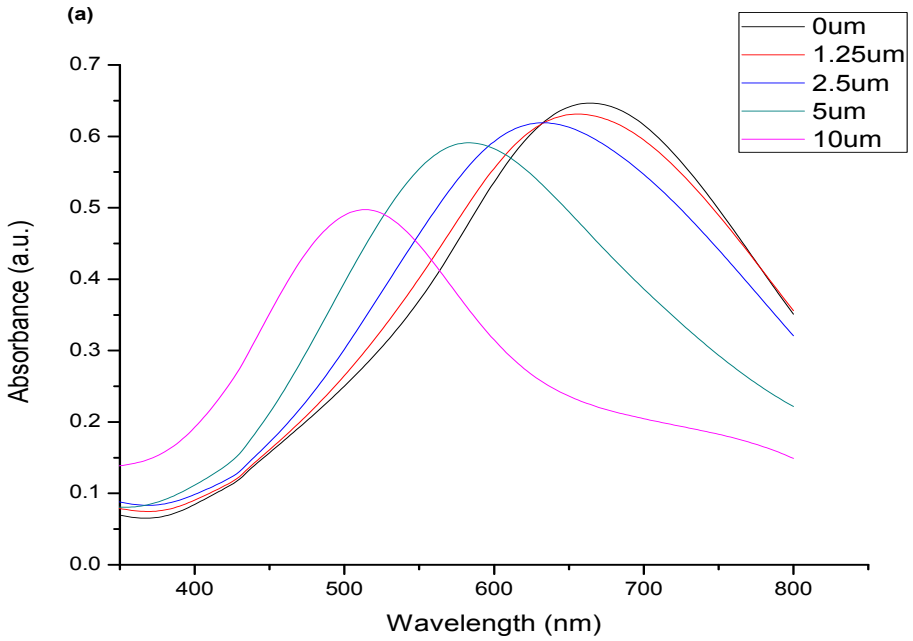

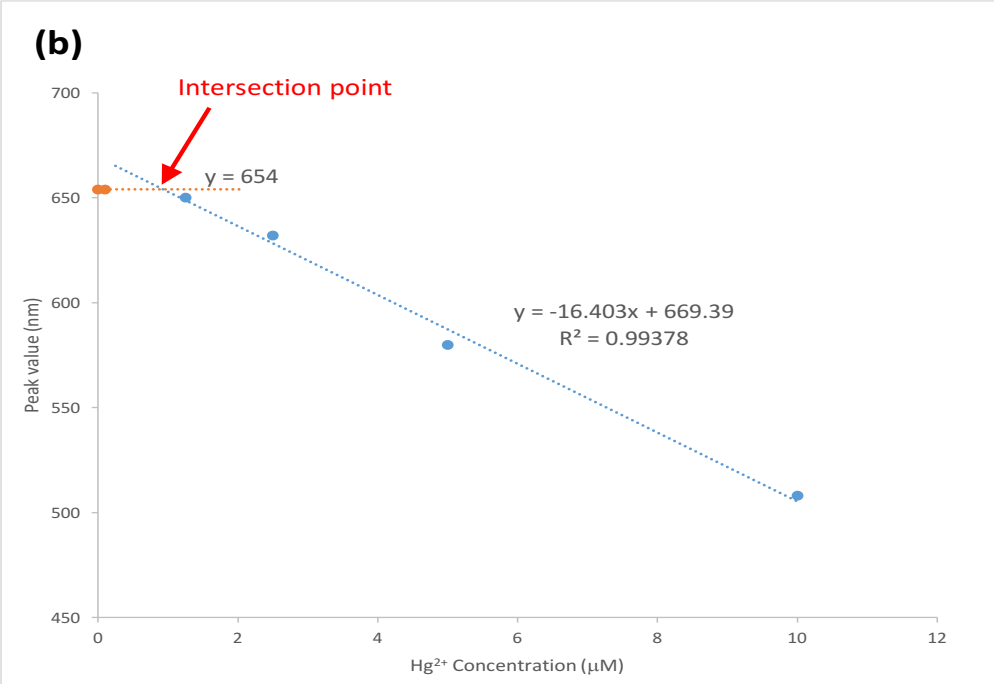

Figure 4.7 (a) UV-Vis Spectroscopy of AgNPs in the presence of different concentrations of Hg^{2+}. (b) Detection of minimum effective concentration (MEC) by linear

fitting of peak value changes of AgNPs in the different concentration of Hg^{2+}.

4.4.3 EDTA Inhibited Assay

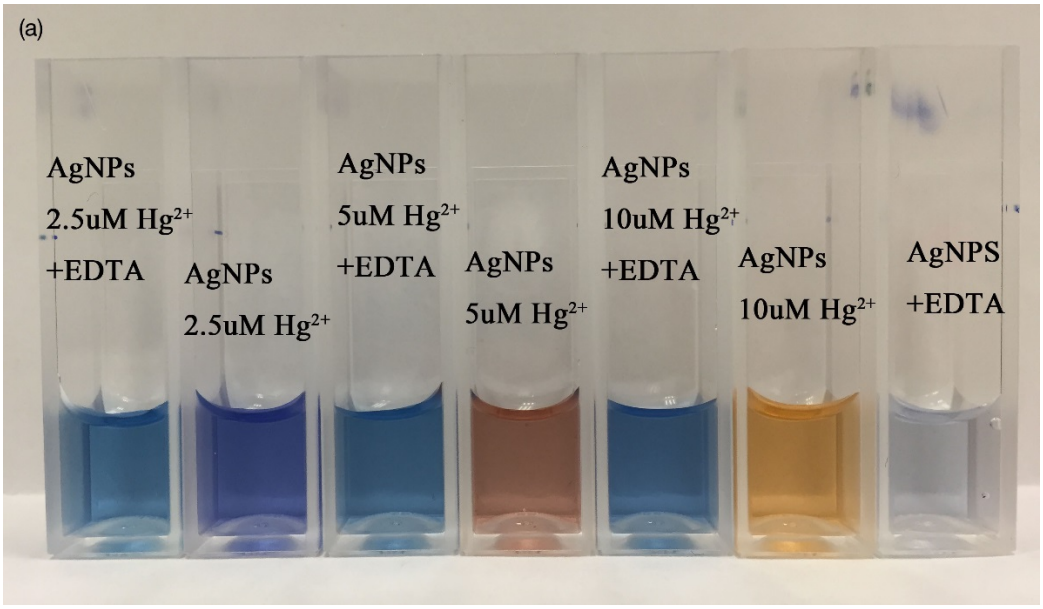

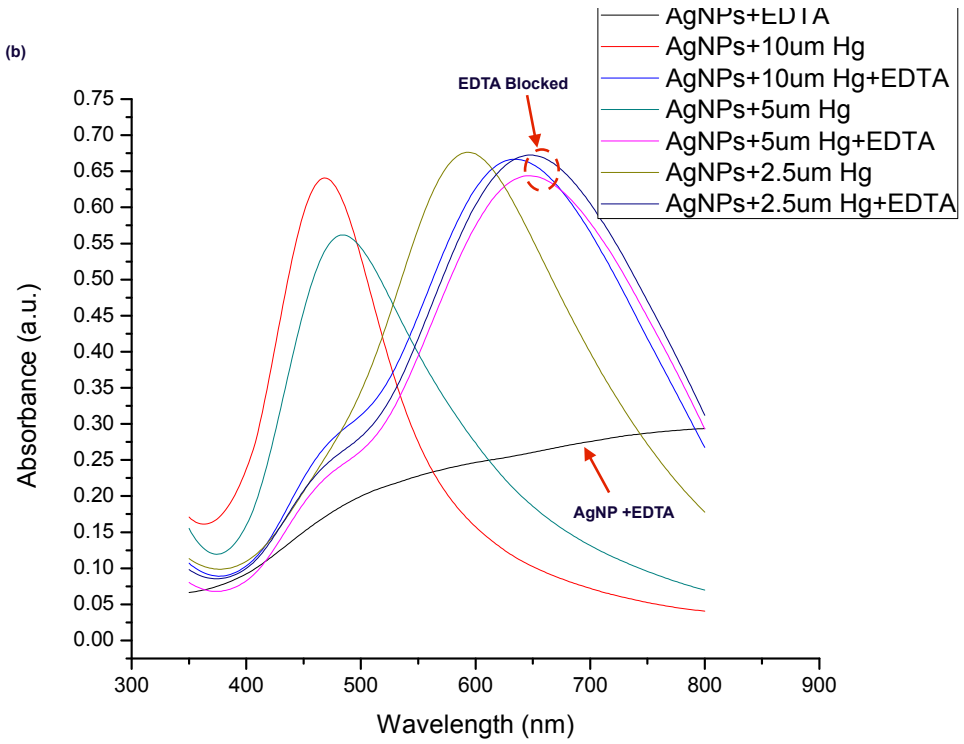

Figure 4.8 (a) Photograph of EDTA inhibited ability. (b) UV-Vis Spectroscopy of EDTA inhibited ability with different concentration of Hg^{2+}.

In this research, an EDTA block assay was performed using three different concentrations of Hg^{2+} solutions. As shown in Figure 4.8, AgNPs can react with EDTA when Hg^{2+} is absent from the solution. However, as evidenced by the lack of changes in the absorption spectra, when Hg^{2+} was present in the solution, EDTA reacted with Hg^{2+} and prevented Hg^{2+} from causing the aggregation of AgNPs. The visible color change with corresponding absorption spectral changes observed in the EDTA block assay provides evidence of the inhibition of AgNP aggregration in the presence of Hg^{2+} and EDTA compared to the presence of Hg^{2+} alone. The EDTA inhibited assay proves that AgNPs could be used to detect Hg^{2+}, likely because of the redox reaction between Ag(0) and Hg^{2+}. In some additional work, EDTA was added after AgNP-Hg^{2+} experiments. However, the AgNPs could not be recovered, which differs from the results reported from another study (Shellaiah, Simon, Sun, & Ko, 2016).

4.4.4 pH Effect

In order to identify the effect and optimal pH range of AgNPs for detecting Hg^{2+} effectively, phosphate buffer solutions were freshly prepared from pH 5 to 10 at 10 μM Hg^{2+}, which was selected to ensure that there was sufficient mercury ion in solution. Different pH values can affect the stability of AgNPs in solution and cause some aggregation of the particles. Therefore, the changes in the peak wavelength of AgNPs-Hg^{2+} in different pH buffer solutions were compared with AgNPs alone in buffer solutions. Figure 4.9 presents the change in peak wavelength for AgNPs in different pH buffers over a 5 min period. To determine the optimal pH

ranges, the absolute value of the slope of peak wavelength versus time was considered as the parameter to compare. In Figure 4.10, it is clearly shown that the slopes of AgNPs peak shift in the range of pH 7.5 to10 (basic conditions) is smaller than those under acidic conditions. Furthermore, the absolute slope value of the AgNPs-Hg^{2+} combination steadily increases as the pH increases, which indicates that Hg^{2+} is better able to cause AgNPs aggregation in basic conditions. Additionally, in basic conditions the slope value difference between AgNPs and AgNPs-Hg^{2+} is two times than those in acidic conditions. Additionally, Figure 4.10 also shows that AgNPs can aggregated under pH7, and the components of phosphate buffer in acidic condition might affect the Hg^{2+}. Thus, the optimal pH range for Hg^{2+} detection is from pH 7.5 to 10.

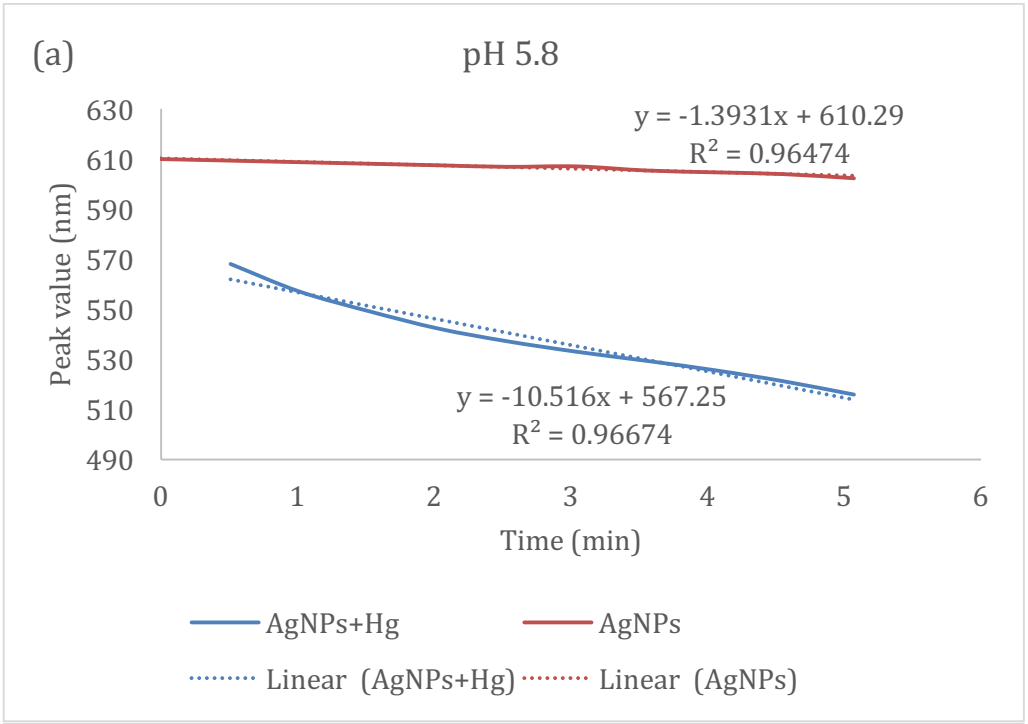
(a)
pH 5.8
y = -1.3931x + 610.29
R² = 0.96474
y = -10.516x + 567.25
R² = 0.96674
Peak value (nm)
630
610
590
570
550
530
510
490
0
1
2
3
4
5
6
Time (min)
AgNPs+Hg
AgNPs
Linear (AgNPs+Hg)
Linear (AgNPs)

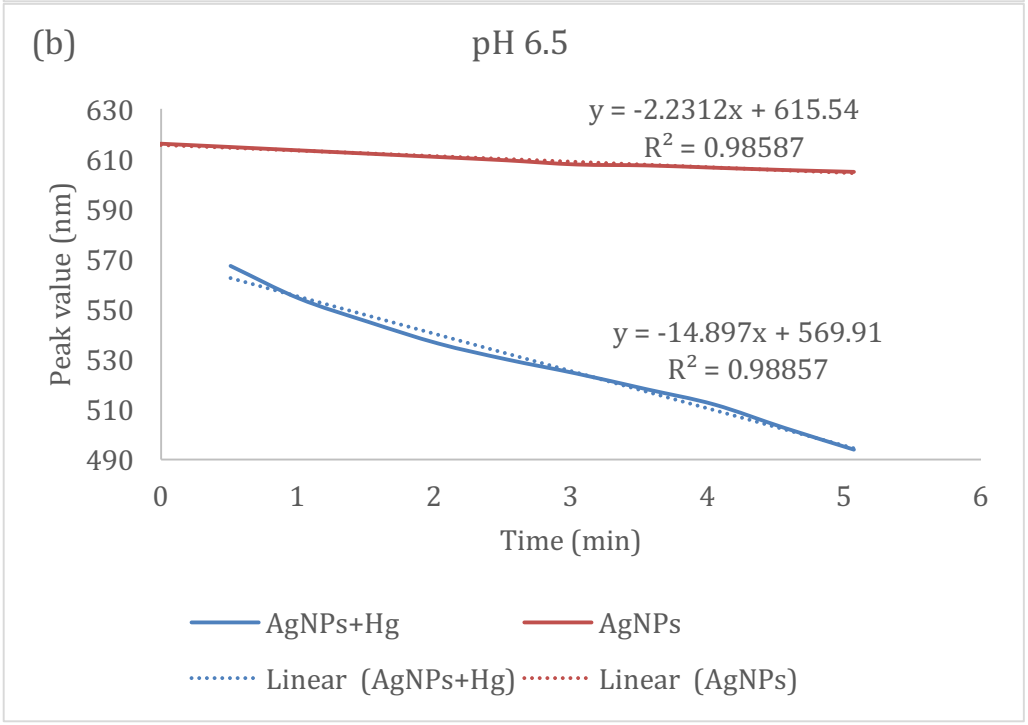
(b)
pH 6.5
y = -2.2312x + 615.54
R² = 0.98587
y = -14.897x + 569.91
R² = 0.98857
Peak value (nm)
630
610
590
570
550
530
510
490
0
1
2
3
4
5
6
Time (min)
AgNPs+Hg
AgNPs
Linear (AgNPs+Hg)
Linear (AgNPs)

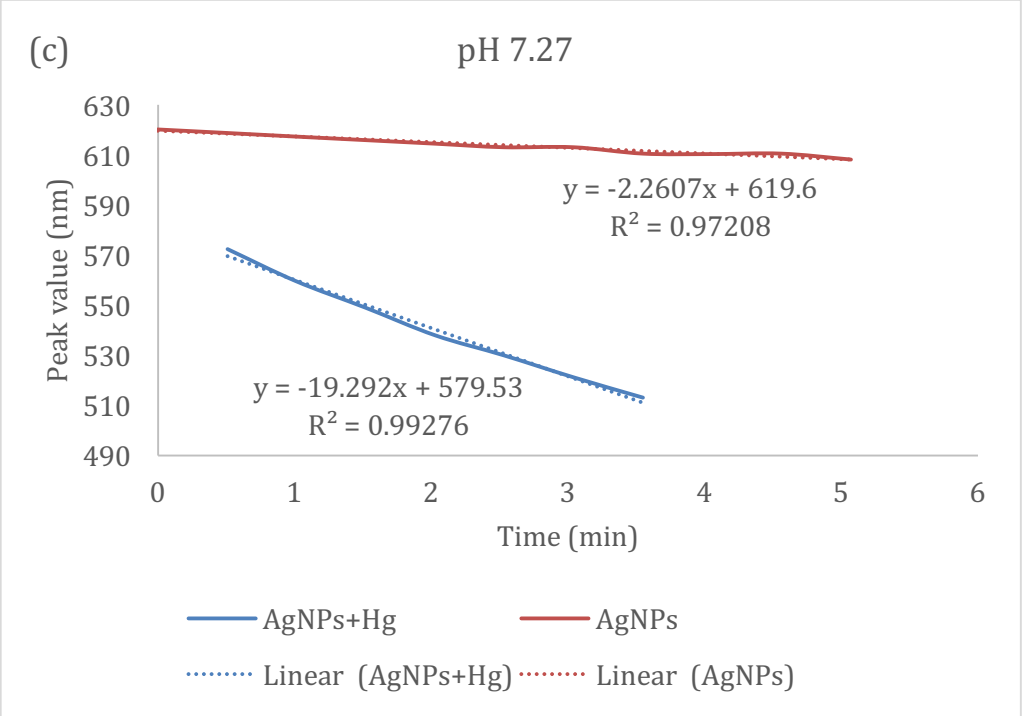
(c)
pH 7.27
Peak value (nm)
630
610
590
570
550
530
510
490
0
1
2
3
4
5
6
Time (min)
y = -2.2607x + 619.6
R² = 0.97208
y = -19.292x + 579.53
R² = 0.99276
AgNPs+Hg
AgNPs
Linear (AgNPs+Hg)
Linear (AgNPs)

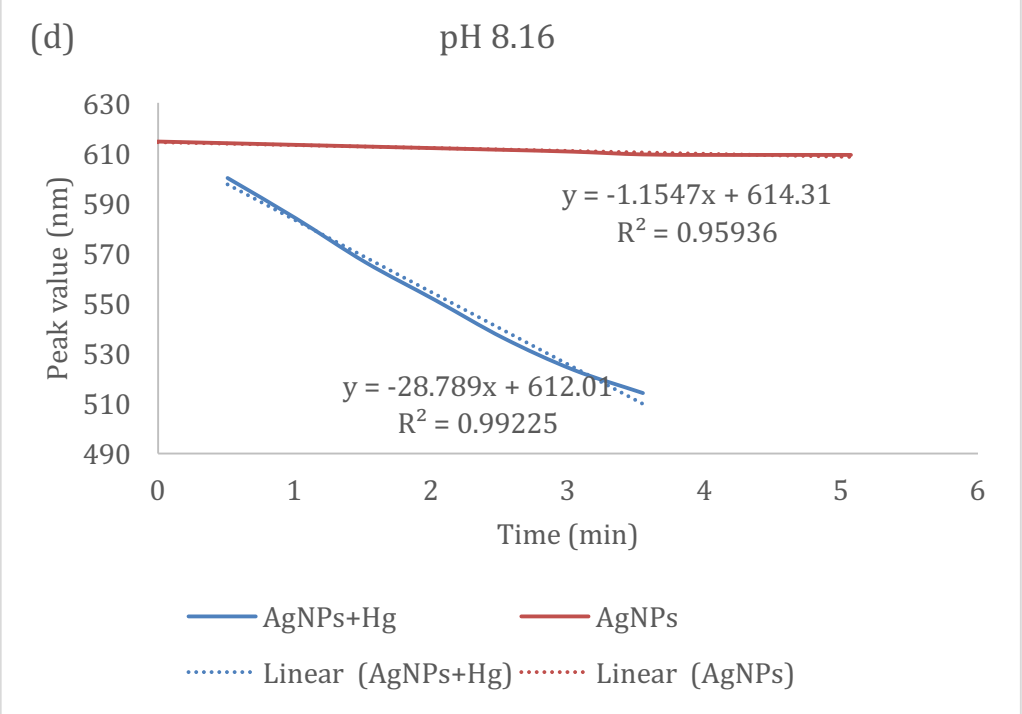
(d)
pH 8.16
Peak value (nm)
630
610
590
570
550
530
510
490
0
1
2
3
4
5
6
Time (min)
y = -1.1547x + 614.31
R² = 0.95936
y = -28.789x + 612.01
R² = 0.99225
AgNPs+Hg
AgNPs
Linear (AgNPs+Hg)
Linear (AgNPs)

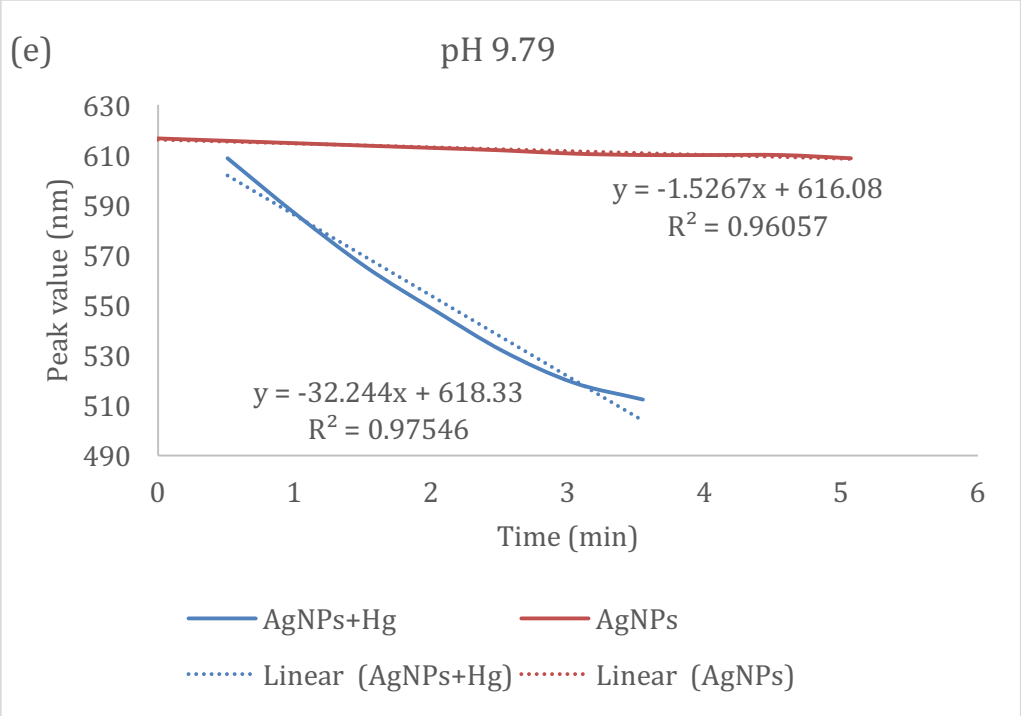

Figure 4.9 The peak shifts for AgNPs-Hg^{2+} and AgNPs in different pH buffer solutions, (a) pH 5.8 (b) pH 6.5 (c) pH 7.27 (d) pH 8.16 (e) pH 9.79.

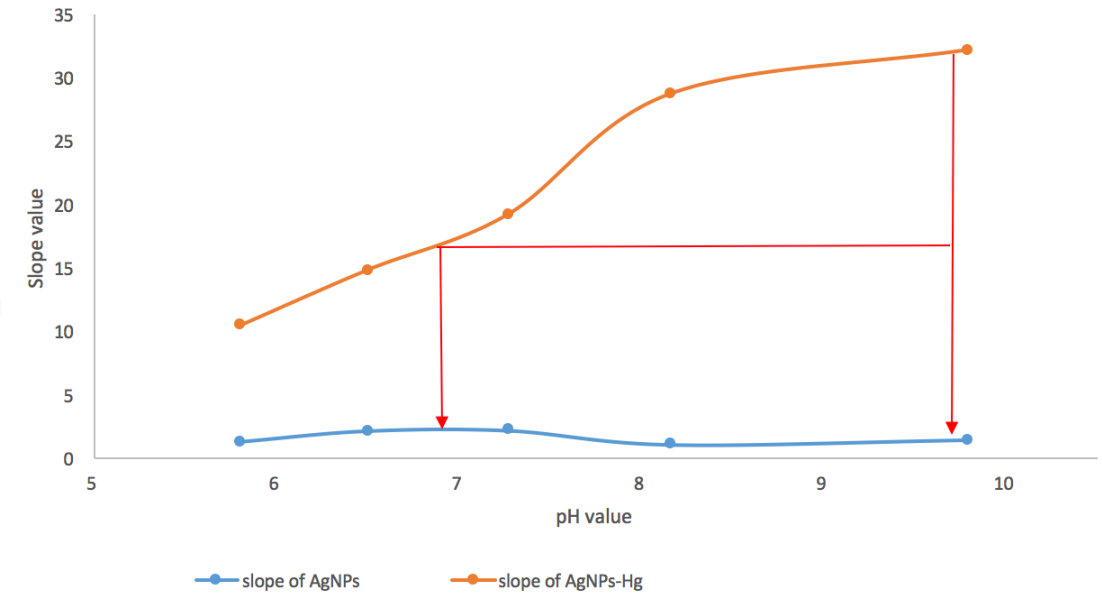

Figure 4.10 pH effects on the initial rate of absorption peak shift of AgNPs in the absence and presence of Hg^{2+} at 10 μM.

4.4.5 Real Sample Study

To confirm the AgNPs selectivity for Hg^{2+} and to examine the possible interference of other ions, laboratory tap water was collected for study and filtered through a 0.2 μm membrane to remove bacteria and particulates that might interfere with the reaction. Then Hg^{2+} was spiked into filtered tap water to fix the final concentration at the following values: 10 μM, 5 μM, 2.5 μM, and 1.25 μM. In Figure 4.11, the results demonstrate that the ability of the AgNPs to detect Hg^{2+} ions was influenced by the ions in tap water, but in spite of this the AgNPs still could target Hg^{2+} because of a color change, as previously observed in DI water for AgNPs in the presence of Hg^{2+}, was easily observed. However, the aggregation phenomenon of AgNPs-Hg^{2+} in tap water showed an opposite effect versus that in DI water. In DI water the concentration with the largest effect is 10 μM, but in tap water the most effective concentration was 1.25 μM, which is close to the MEC measured in DI water.

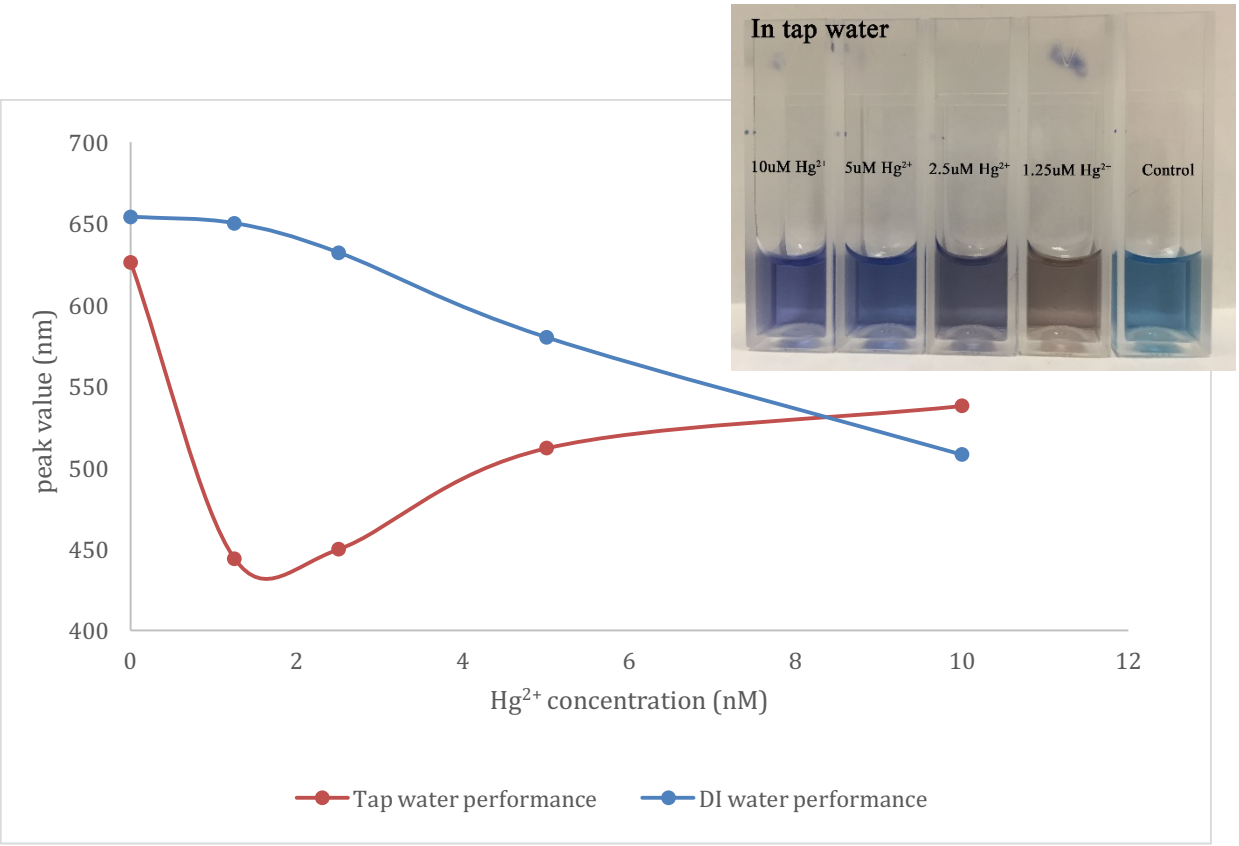

Figure 4.11 AgNPs performed in tab water and DI water with different concentration of Hg^{2+}.

This phenomenon could be explained with the concepts illustrated in the Figure 4.12. In DI water, there are very few free ions, thus Hg^{2+} will first break the PVP (AgNPs) stabilizerchain, then attach on the surface of AgNPs. That is why sufficient Hg^{2+}, like 10 μM, could give a better result than lower concentrations in DI water. However, tap water contains a large amount of ions, and those ions could break PVP chain and allow Hg^{2+} attaching on the AgNPs directly (Figure 4.11 right). Thus, in tap water 1.25 μM could show the best performance. Further research is needed to determine the ratio between PVP and the ions in tap water.

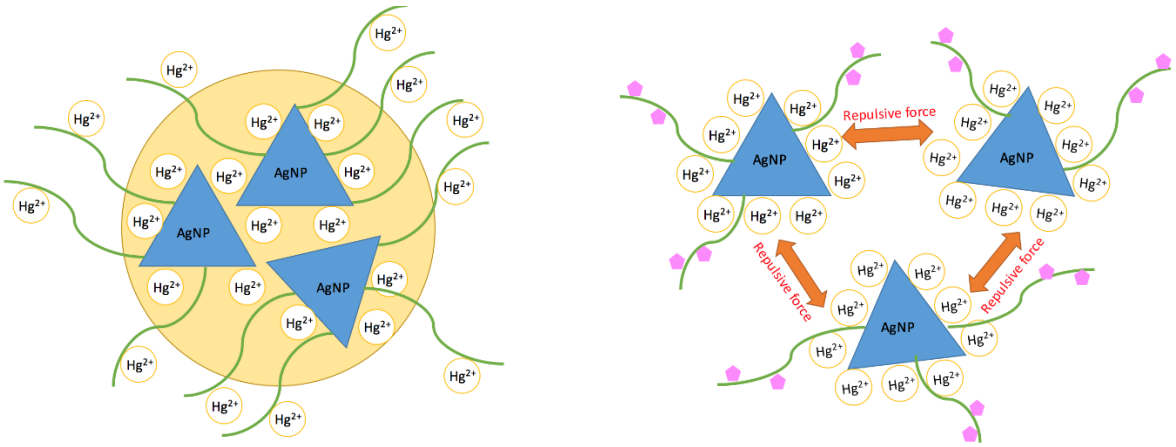

Figure 4.12 Principle of AgNPs-Hg^{2+} aggregation in DI water (left) and tap water (right).

4.5 Summary and Conclusions

A PVP-stabilized triangular AgNPs colorimetric assay provided a fast method for Hg^{2+} detection. These triangular AgNPs were synthesized with chemical methods and their application as a sensitive colorimetric Hg^{2+} probe is reported here for the first time. The results of TEM and DLS indicate that AgNPs are triangular shape and approximately 35 nm in side length. They have intense surface plasmon resonance and negative surface charge (-27.6 mV). The selectivity of AgNPs for Hg^{2+} was characterized via TEM and DLS, it is clearly shown that Hg^{2+} acts as a bridge to induce AgNPs aggregation, and a minimum effective concentration of Hg^{2+} detected was found at 0.938 μM. The optimal working pH range of AgNPs for Hg^{2+} identification is pH 7 to 10. From a spiked tap water study, AgNPs were slightly disturbed by ions in tap water, but the selectivity towards Hg^{2+} was exceptional.

Chapter 5

Conclusions and Recommendations

5.1 Conclusions

The study in this thesis highlighted the manipulation of silver nanoparticles and their properties for application in a colorimetric assay for heavy metal detection. Furthermore, the process of silver nanoparticles binding with Poly-L-lysine was studied, and the antibacterial activity was evaluated. In this study, silver nanoparticles showed a strong antibacterial ability, and were non-toxic towards mammalian cells. The results of heavy metal detection also indicated the unique physical and chemical properties of silver nanoparticles. The marked features of this work could be summarized as follow:

1. The triangular AgNPs were characterized via TEM, UV-Vis, DLS and zeta-potential. It was proven that triangular AgNPs have a negative surface charge. Poly-L-lysine functionalized AgNPs easily changed the surface charge from negative to positive, thereby apparently increasing the antibacterial activity.

2. The antibacterial tests evaluated the activities of AgNPs-PLL against four bacterial strains, gram-negative bacteria *E. coli* and *P. aeruginosa*, and gram-positive bacteria *B. subtilis* and *S. aureus*. The results showed a more than 90% decrease of bacterial viability within 4 hours after applying AgNPs-PLL in 4 hours.

3. The colorimetric assay for detection of mercury using PVP stabilized triangular AgNPs showed that the optimal working pH range of these AgNPs was from pH 7.5 to pH 10,

and the minimum effective concentration (MEC) for determining mercury in water was 0.938 μM. Additionally, the color change could be visually observed.

4. The real sample study of selective detection of mercury in tap water by PVP stabilized triangular AgNPs indicated that AgNPs were slightly affected by ions in the tap water, but the sensitivity towards Hg^{2+} was exceptional (the most effective concentration is 1.25μM).

5.2 Recommendations for Future Work

The triangular silver nanoparticles undoubtedly have significant physiochemical properties, and can especially be manipulated with polymers for application in antibacterial applications. Thus, some of the study presented here can be extended in certain major directions. For example, using AgNP-PLL in cleaning and disinfection products, such as surface wipes, and anti-bacterial spray. In addition, the further research of anti-fungal and antiviral activities of AgNPs-PLL also need to be evaluated.

The AgNPs rapid colorimetric detection of mercury was based on the AgNPs structure sensitive property. Hence, the AgNPs morphology might affect the heavy metal detection activity. Therefore, manipulating the AgNPs morphologies should be investigated. AgNPs were found to be slightly affected by other ions in tap water, and increasing the amount of PVP might help to solve this problem. Therefore, determining the optimal ratio of AgNPs and PVP is important for improving the heavy metal detection and minimizing interferences in the sample. For further enhancing the applications of AgNPs, they could be applied on lateral flow assay for developing a facile, rapid, sensitive and cost-effective protocol, but AgNPs should be modified by adding surfactant to guarantee or stabilize the activity.

Reference

Abdel-Raouf, N., Al-Enazib, N. M., & Ibraheem, I. B. (2013). Green biosynthesis of gold nanoparticles using Galaxaura elongata and characterization of their antibacterial activity. *Arabian Journal of Chemistry*, 1-11.

Abid, J. P., Wark, A. W., Brevet, P. F., & Girault, H. H. (2002). Preparation of silver nanoparticles in solution from a silver salt by laser irradiation. *The Royal Society of Chemistry*, 792-793.

Ahmed, S., Annu, Ikram, S., & Yudha S., S. (2016, August). Biosynthesis of gold nanoparticles: A green approach. *Journal of Photochemistry and Photobiology B: Biology, 161*, 141-153.

Armendariz, V., Herrera, I., Peralta-Videa, J. R., Jose-Yacaman, M., Troiani, H., Santiago, P., & Gardea-Torresdey, J. L. (2004). Size controlled gold nanoparticle formation by Avena sativa biomass: use of plants in nanobiotechnology. *Journal of Nanoparticle Research*, 377-382.

Arunkumar, P., Thanalakshmi, M., Kumar, P., & Premkumar, K. (2013). Micrococcus luteus mediated dual mode synthesis of gold nanoparticles : involvement of extracellular amylase and cell wall teichuronic acid. *Colloids Surf. B Biointerfaces, 103*, 517-522.

Ateeq, M., Shah, M. R., Ain, N., Bano, S., Anis, I., Lubna, . . . Naz, S. S. (2015). Green synthesis and molecular recognition ability of patuletin coated gold nanoparticles. *Biosensors and Bioelectronics, 63*, 499-505.

Badawy, A. M., Luxton, T. P., Silva, R. G., Scheckel, K. G., Suidan, M. T., & Tolaymat, T. M. (2010). Impact of Environmental Conditions (pH, Ionic Strength, and Electrolyte Type)

on the Surface Charge and Aggregation of Silver Nanoparticles Suspensions. *Environ. Sci. Technol., 44*, 1260-1266.

Bax, R. P. (1997). Antibiotic Resistance: A View from the Pharmaceutical Industry. *Clinical Infectious Disease, 24*(1), 151-153.

Beveridgr, T. J. (1999). Structures of Gram-Negative Cell Walls and Their Derived Membrane Vesicles. *JOURNAL OF BACTERIOLOGY*, 4725–4733.

Brause, R., Möltgen, H., & Kleinermanns, K. (2002). Characterization of laser-ablated and chemically reduced silver colloids in aqueous solution by UV/VIS spectroscopy and STM/SEM microscopy. *Applied Physics B, 75*(6), 711-716.

Buwa, L., & Staden, J. v. (2006). Antibacterial and antifungal activity of traditional medicinal plants used against venereal diseases in South Africa. *Journal of Ethnopharmacology, 103*(1), 139–142.

Balogh, L., Swanson, D., Tomalia, D., Hagnauer, G., & McManus, A. (2001). Dendrimer–silver complexes and nanocomposites as antimicrobial agents. *Nano Lett*, 18-21.

Basavegowda, N., Idhayadhulla, A., & Lee, Y. K. (2014). Phyto-synthesis of gold nanoparticles using fruit extract of Hovenia dulcis and their biological activities. *Industrial Crops and Products, 52*, 745-751.

Brust, M., Walker, M., Bethell, D., Schiffrin, D. J., & Whyman, R. (1994). Synthesis of thiol-derivatised gold nanoparticles in a two-phase Liquid–Liquid system. *J. Chem. Soc., Chem. Commun*, 801-802.

Bridle, H., Balharry, D., Gaiser, B., & Johnston, H. (2015). Exploitation of Nanotechnology for the Monitoring of Waterborne Pathogens: State-of-the-Art and Future Research Priorities. *Environ. Sci. Technol., 49*, 10762−10777.

Burrell, R., Heggers, J., Davis, G., & Wrigh, J. B. (1999). Efficacy of Silver-Coated Dressings as Bacterial Barriers in a Rodent Burn Sepsis Model. *Wounds, 11*(4), 64-71.

Carvalho, C. M., Chew, E. H., Hashemy, S. I., Lu, J., & Holmgren, A. (2008). Inhibition of the human thioredoxin system. A molecular mechanism of mercury toxicity. *J Biol Chem, 283*(18), 11913-23.

Crabtree, J. H., Burchette, R. J., Siddiqi, R. A., Huen, I. T., Handott, L. L., & Fishman, A. (2003). The efficacy of silver-ion implanted catheters in reducing peritoneal dialysis-related infections. *Perit Dial Int*, 368 - 74.

Chai, F., Wang, C., Wang, T., Li, L., & Su, Z. (2010). Colorimetric Detection of Pb2+ Using Glutathione Functionalized Gold Nanoparticles. *Applied materials and interfaces*, 1466-1467.

Chen, Z., Liu, R., Wang, S., Qu, C., Chen, L., & Wang, Z. (2013). Colorimetric sensing of copper(II) based on catalytic etching of gold nanorods. *RSC Advances*, 13318-13323.

Chena, J., Wang, J., Zhang, X., & Jin, Y. (2008). Microwave-assisted green synthesis of silver nanoparticles by carboxymethyl cellulose sodium and silver nitrate. *Materials Chemistry and Physics, 108*(2-3), 421-424.

Chun, A. L. (2009). Silver plates: Sizing and shaping with light. *Nature Nanotechnology*, 114.

Clarkson, T. W., Magos, L., & Myers, G. J. (2003). The Toxicology of Mercury — Current Exposures and Clinical Manifestations. *The new england journal of medicine*, 1731-7.

Corbierre, M. K., & Lennox, R. B. (2005). Preparation of Thiol-Capped Gold Nanoparticles by Chemical Reduction of Soluble Au(I)−Thiolates. *Chem. Mater.*, 5691-5696.

Cowan, M., Abshire, K., Houk, S., & Evans, S. (2003). Antimicrobial efficacy of a silver-zeolite matrix coating on stainless steel. *J Ind Microbiol Biotechnol*, 102-106.

Davies, J., & Wright, G. D. (1997). Bacterial resistance to aminoglycoside antibiotics. *Trends in Microbiology, 5*(6), 234-240.

Dong, P. V., Ha, C. H., Binh, L. T., & Kasbohm, J. (2012). Chemical synthesis and antibacterial activity of novel-shaped silver nanoparticles. *International Nano Letters, 2*(1), 1-9.

Dai, B., Cao, M., Fang, G., Liu, B., Dong, X., Pan, M., & Wang, S. (2012). Schiff base-chitosan grafted multiwalled carbon nanotubes as a novel solid-phase extraction adsorbent for determination of heavy metal by ICP-MS. *Journal of Hazardous Materials, 219–220*, 103–110.

Darbha, G. K., Singh, A. K., Rai, U. S., Yu, E., Yu, H., & Ray, P. C. (2008). Selective Detection of Mercury (II) Ion Using Nonlinear Optical Properties of Gold Nanoparticles. *J. Am. Chem. Soc., 130*(25), 8038-8043.

Duan, J., Yin, H., Wei, R., & Wang, W. (2014). Facile colorimetric detection of Hg2+ based on anti-aggregation of silver nanoparticles. *Biosens. Bioelectron, 57*, 139-142.

Djedjibegovic, J., Larssen, T., Skrbo, A., Marjanović, A., & Sober, M. (2012). Contents of cadmium, copper, mercury and lead in fish from the Neretva river (Bosnia and Herzegovina) determined by inductively coupled plasma mass spectrometry (ICP-MS). *Food Chemistry, 131*(2), 469-476.

Elechiguerra, J. L., Burt, J. L., Morones, J. R., Camacho-Bragado, A., Gao, X., Lara, H. H., & Yacaman, M. J. (2005). Interaction of silver nanoparticles with HIV-1. *Journal of Nanobiotechnology*, 1-10.

Esumi, K., Matsuhisa, K., & Torigoe, K. (1995). Preparation of Rodlike Gold Particles by UV Irradiation Using Cationic Micelles as a Template. *Langmuir, 11*, 3285-3287.

Eustis, S., Krylova, G., Eremenko, A., Smirnova, N., Schill, A., & El-Sayed, M. (2005). Growth and fragmentation of silver nanoparticles in their synthesis with a fs laser and CW light by photo-sensitization with benzophenone. *Photochem. Photobiol. Sci., 4*, 154-159.

Evanoff, D. D., & Chumanov, G. (2004). Size-Controlled Synthesis of Nanoparticles. 1. "Silver-Only" Aqueous Suspensions via Hydrogen Reduction. *J. Phys. Chem. B, 108*(37), 13948-13956.

Eustis, S., Krylova, G., Eremenko, A., Smirnova, N., Schill, A. W., & El-Sayed, M. (2005). Growth and fragmentation of silver nanoparticles in their synthesis with a fs laser and CW light by photo-sensitization with benzophenone. *Photochem. Photobiol. Sci., 4*, 154-159.

Fayaz, A. M., Balaji, K., Girilal, M., Yadav, R., Kalaichelvan, P. T., & Venketesan, R. (2010). Biogenic synthesis of silver nanoparticles and their synergistic effect with antibiotics: a study against gram-positive and gram-negative bacteria. *Nanomedicine: Nanotechnology, Biology, and Medicine, 6*, 103–109.

Fayaz, A., Girilal, M., Rahman, M., Venkatesan, R., & Kalaichelvan, P. T. (2011). Biosynthesis of silver and gold nanoparticles using thermophilic bacterium Geobacillus stearothermophilus. *Process Biochem., 46*, 1958-1962.

Fu, R., Li, J., & Yang, W. (2012). Aggregation of glutathione-functionalized Au nanoparticles induced by Ni2+ ions. *J Nanopart Res*, 1-8.

Fan, Y., Liu, Z., Wang, L., & Zhan, J. (2009). Synthesis of Starch-Stabilized Ag Nanoparticles and Hg2+ Recognition in Aqueous Media. *Nanoscale Res Lett*, 1230-1235.

Faraji, M., Yamini, Y., Saleh, A., Rezaee, M., Ghambarian, M., & Hassani, R. (2010). A nanoparticle-based solid-phase extraction procedure followed by flow injection inductively coupled plasma-optical emission spectrometry to determine some heavy metal ions in water samples. *Analytica Chimica Acta, 659*(1-2), 172-177.

Ganeshkumar, M., Sathishkumar, M., Ponrasu, T., Girija, M., & Suguna, L. (2013). Spontaneous ultra fast synthesis of gold nanoparticles using Punica granatum for cancer targeted drug delivery. *Colloids Surf. B Biointerfaces, 106*, 208-216.

Geethalakshmi, R., & L., S. D. (2013). Characterization and antimicrobial activity of gold and silver nanoparticles synthesized using saponin isolated from Trianthema decandra L. *Industrial Crops and Products, 51*, 107-115.

Godwin, H. A. (2001). The biological chemistry of lead. *Current Opinion in Chemical Biology, 5*(2), 223-227.

Guan, J., Wang, Y. C., & Gunasekaran, S. (2015). Using L-arginine-functionalized gold nanorods for visible detection of mercury(II) ions. *J. Food Sci,*, 828-833.

Gupta, A., & Silver, S. (1998). Molecular Genetics: Silver as a biocide: Will resistance become a problem? *Nature Biotechnology*, 888.

Ghafari-Nazari, A., Moztarzadeh, F., Rabiee, S. M., Rajablo, T., & Moza, M. (2012). Antibacterial activity of silver photodeposited nepheline thin film coatings. *Ceramics International, 38*, 5445–5451.

Gibbins, B., & Warner, L. (2005). The role of antimicrobial silver nanotechnology. *Med Device Diagnostic Indust Mag*(1), 1-2.

Guzman, M., Dille, J., & Godet, S. (2012). Synthesis and antibacterial activity of silver nanoparticles against gram-positive and gram-negative bacteria. *Nanomedicine: Nanotechnology, Biology, and Medicine*(8), 37-45.

Health Canada. (2013, June 27). *Food Additives*. Retrieved from Health Canada: www.hc-sc.gc.ca

Hamouda, T., Myc, A., Donovan, B., Shih, A., Reuter, J., & Baker, J. (2001). A novel surfactant nanoemulsion with a unique non-irritant topical antimicrobial activity against bacteria, enveloped viruses and fungi. *Microbiol. Release,*, 1-7.

He, S., Guo, Z., Zhang, Y., Zhang, S., Wang, J., & Gu, N. (2007). Biosynthesis of gold nanoparticles using the bacteria Rhodopseudomonas capsulata. *Materials Letters, 61*, 3984-3987.

Henglein, A. (1993). Physicochemical properties of small metal particles in solution: "microelectrode" reactions, chemisorption, composite metal particles, and the atom-to-metal transition. *J. Phys. Chem., 97*(21), 5457-5471.

Huang, H., & Yang, X. (2004). Synthesis of polysaccharide-stabilized gold and silver nanoparticles: a green method. *Carbohydrate Research, 339*, 2627-2631.

Husseiny, M., El-Aziz, M. A., Badr, Y., & Mahmoud, M. (2007). Biosynthesis of gold nanoparticles using Pseudomonas aeruginosa. *Spectrochimica Acta Part A, 67*, 1003-1006.

Huang, X., & Choi, Y. (2007). Chemical sensors based on nanostructured materials. *Sensors and Actuators B, 122*, 659-671.

Haruta, M. (2002). Catalysis of Gold Nanoparticles Deposited on Metal Oxides. *Cattech, 6*(3), 102-115.

Inbakandan, D., Venkatesan, R., & Khan, S. R. (2010). Biosynthesis of gold nanoparticles utilizing marine sponge Acanthella elongata (Dendy, 1905). *Colloids and Surfaces B: Biointerfaces, 81*(2), 634-639.

Inoue, Y., Hoshino, M., Takahashi, H., Noguchi, T., Murata, T., Kanzaki, Y., . . . Sasatsu, M. (2002). Bactericidal activity of Ag–zeolite mediated by reactive oxygen species under aerated conditions. *Journal of Inorganic Biochemistry, 92*(1), 37-42.

Jain, P. K., Huang, X., El-Sayed, I., & El-Sayed, M. A. (2007). Review of Some Interesting Surface Plasmon Resonance-enhanced Properties of Noble Metal Nanoparticles and Their Applications to Biosystems. *Plasmonics*, 107-118.

Jana, N. R., Gearheart, L., & Murphy, C. J. (2001). Wet Chemical Synthesis of High Aspect Ratio Cylindrical Gold Nanorods. *J. Phys. Chem. B*, 4065-4067.

Jayaseelan, C., Ramkumar, R., Rahuman, A., & Perumal, P. (2013). Green synthesis of gold nanoparticles using seed aqueous extract of Abelmoschus esculentus and its antifungal activity. *Industrial Crops and Products, 45*, 423-429.

Ji, X., Song, X., Li, J., Bai, Y., Yang, W., & Peng, X. (2007). Size Control of Gold Nanocrystals in Citrate Reduction: The Third Role of Citrate. *J. Am. Chem. Soc., 129*(45), 13939-13948.

Johnson, E. R., Wallace, P. J., Cashman, K. V., Granados, H. D., & Kent, A. G. (2008). Magmatic volatile contents and degassing-induced crystallization at Volcán Jorullo, Mexico: Implications for melt evolution and the plumbing systems of monogenetic volcanoes. *Earth and Planetary Science Letters , 269*(3-4), 478–487.

Kalishwaralal, K., Deepak, V., Pandian, S. R., Kottaisamy, M., BarathManiKanth, S., Kartikeyan, B., & Gurunathan, S. (2010). Biosynthesis of silver and gold nanoparticles using Brevibacterium casei. *Colloids and Surfaces B: Biointerfaces, 77*, 257-262.

Karuppaiya, P., Satheeshkumar, E., Chao, W., Kao, L., Chen, E., & Tsay, H. (2013). Anti-metastatic activity of biologically synthesized gold nanoparticles on human fibrosarcoma cell line HT-1080. *Colloids Surf. B Biointerfaces, 110*, 163-170.

Khalil, M. M., Ismail, E. H., & El-Magdoub, F. (2012). Biosynthesis of Au nanoparticles using olive leaf extract : 1st Nano Updates. *Arabian Journal of Chemistry, 5*(4), 431-437.

Kim, H. N., Ren, W. X., Kim, J. S., & Yoon, J. (2012). Fluorescent and colorimetric sensors for detection of lead, cadmium, and mercury ions. *Chemical Society Reviews, 41*, 3013-3432.

Kim, J. S., Kuk, E., Yu, K. N., Kim, J., Park, S. J., Lee, H. J., . . . Cho, M. (2007). Antimicrobial effects of silver nanoparticles. *Nanomedicine: Nanotechnology, Biology and Medicine, 3*(1), 95-101.

Kim, K. J., Sung, W. S., Moon, S. K., Choi, J. S., Kim, J. G., & Lee, D. G. (2008). Antifungal effect of silver nanoparticles on dermatophytes. *J Microbiol Biotechnol*, 1482-1484.

Krpetic, Z. G. (2012). Importance of Nanoparticle Size in Colorimetric and SERS-Based Multimodal Trace Detection of Ni(II) Ions with Functional Gold Nanoparticles. *Small*, 707-714.

Kumar, V. G., Gokavarapu, S. D., Rajeswari, A., Dhas, T. S., Karthicka, V., Kapadia, Z., . . . Sinha, S. (2011). Facile green synthesis of gold nanoparticles using leaf extract of antidiabetic potent Cassia auriculata. *Colloids and Surfaces B: Biointerfaces, 87*(1), 159-163.

Kvitek, L., Panacek, A., Soukupova, J., Kolar, M., Vecerova, R., Prucek, R., . . . Zboril, R. (2008). Effect of surfactants and polymers on stability and antibacterial activity of silver nanoparticles (NPs). *J Phys Chem C*, 5825-5834.

Kelly, J., Keegan, G., & Brennan-Fournet, M. (2012). Triangular Silver Nanoparticles: Their Preparation, Functionalisation and Properties. *CTA PHYSICA POLONICA A,*, 337-344.

Kerker, M. (1985). The optics of colloidal silver: something old and something new. *Journal of Colloid and Interface Science, 105*(2), 297-314.

Kim, J. S., Kuk, E., Yu, K. N., Kim, J., Park, S., Lee, H., . . . Cho, M. (2007). Antimicrobial effects of silver nanoparticles. *Nanomedicine: Nanotechnology, Biology, and Medicine*(7), 95–101.

Klasen, H. (2000). A historical review of the use of silver in the treatment of burns. II. Renewed interest for silver. *Burns, 26*(2), 131–138.

Krikorian, V., Kurian, M., Galvin, M. E., Nowak, A. P., Deming, T. J., & Pochan, D. J. (2002). Polypeptide-Based Nanocomposite: Structure and Properties of Poly (L-lysine)/Na+-Montmorillonite. *Journal of Polymer Science: Part B: Polymer Physics, 40*, 2579–2586.

Kumar, R., & Münstedt, H. (2005). Silver ion release from antimicrobial polyamide/silver composite Pages 2081–2088. *Biomaterials, 26*(14), 2081–2088.

Langford, N. J., & Ferner, R. E. (1999). Toxicity of mercury. *Journal of Human Hypertension, 13*, 651-656.

Li, Y., Cui, L., Li, Q., Jia, L., Xu, Y., Fang, Q., & Cao, A. (2007). Novel Symmetric Amphiphilic Dendritic Poly(L-lysine)-b-Poly(L-lactide)-b-Dendritic Poly(L-lysine) with High Plasmid DNA Binding Affinity as a Biodegradable Gene Carrier. *Biomacromolecules, 8*, 1409-1416.

Lin, S., Chen, L., Huang, L., Cao, S., Luo, X., & Liu, K. (2015). Novel antimicrobial chitosan–cellulose composite films bioconjugated with silver nanoparticles. *Industrial Crops and Products, 70*, 395–403.

Lee, I. S. (2014). Triazole-acetate functionalized gold nanoparticles for colorimetric Pb(II) sensing. *RSC Advances*, 25251-25256.

Lee, J., Han, M. S., & Mirkin, C. A. (2007). Colorimetric Detection of Mercuric Ion (Hg2+) in Aqueous Media using DNA-Functionalized Gold Nanoparticles. *Angew. Chem. Int. Ed, 46*, 4093-4096.

Lee, K., Nagajyothi, P. C., Sreekanth, T. V., & Park, S. (2015). Eco-friendly synthesis of gold nanoparticles (AuNPs) using Inonotus obliquus and their antibacterial, antioxidant and cytotoxic activities. *Journal of Industrial and Engineering Chemistry, 26*, 67-72.

Lee, P., & Meisel, D. (1982). Adsorption and Surface-Enhanced Raman of Dyes on Silver and Gold Sols. *J. Phys. Chem., 86*, 3391-3395.

Li, D., Wieckowska, A., & Willner, I. (2008). Optical Analysis of Hg2+Ions by Oligonucleotide–Gold-NanoparticleHybrids and DNA-Based Machines. *Angew. Chem. Int. Ed, 47*(21), 3927-31.

Li, S., Shen, Y., Xie, A., Yu, X., Qiu, L., Zhang, L., & Zhang, Q. (2007). Green synthesis of silver nanoparticles using Capsicum annuum L. extract. *Green Chemistry*(8), 852-858.

Liau, S., Read, D., Pugh, W. J., Furr, J., & Russell, A. (1997). Interaction of silver nitrate with readily identifiable groups: relationship to the antibacterialaction of silver ions. *Letters in Applied Microbiology, 25*(4), 279-283.

Liu, D., Qu, W., Chen, W., Zhang, W., Wang, Z., & Jiang, X. (2010). Highly Sensitive, Colorimetric Detection of Mercury(II) in Aqueous Media by Quaternary Ammonium Group-Capped Gold Nanoparticles at Room Temperature. *Anal. Chem., 82*(23), 9606-9610.

Lu, L., Sun, R. W., Chen, R., Hui, C., Ho, C. M., Luk, J. M., . . . Che, C. (2008). Silver nanoparticles inhibit hepatitis B virus replication. *Antivir Ther*, 253-262.

Luo, J., Wang, Y., & Tan, K. (2012). Colorimetric detection of mercury(II) based on silver nanoparticles. *Acta Chimi. Sin, 70*, 1945-1949.

Lee, K., & El-Sayed, M. A. (2006). Gold and Silver Nanoparticles in Sensing and Imaging: Sensitivity of Plasmon Response to Size, Shape, and Metal Composition. *J. Phys. Chem. B, 110*(39), 19220-19225.

Li, D., Wieckowska, A., & Willner, I. (2008). Optical Analysis of Hg2+Ions by Oligonucleotide–Gold-NanoparticleHybrids and DNA-Based Machines. *Angew. Chem. Int. Ed, 47*(21), 3927-31.

McFarland, C. N., Bendell-Young, L. I., Guglielmo, C., & Williams, T. D. (2002). Kidney, liver and bone cadmium content in the western sandpiper in relation to migration. *J. Environ. Monit., 4*, 791-795.

Mingorancea, M., Valdés, B., & Oliva, S. R. (2007). Strategies of heavy metal uptake by plants growing under industrial emissions. *Environment International, 33*(4), 514–520.

Manivasagan, P., Venkatesan, J., Kang, K., Sivakumar, K., Park, S., & Kim, S. (2015). Production of alpha-amylase for the biosynthesis of gold nanoparticles using Streptomyces sp. MBRC-82. *International Journal of Biological Macromolecules, 72*, 71-78.

MubarakAli, D., Thajuddina, N., Jeganathan, K., & Gunasekaran, M. (2011). Plant extract mediated synthesis of silver and gold nanoparticles and its antibacterial activity against clinically isolated pathogens. *Colloids and Surfaces B: Biointerfaces, 85*, 360-365.

Muniyappan, N., & Nagarajan, N. (2014). Green synthesis of gold nanoparticles using Curcuma pseudomontana essential oil, its biological activity and cytotoxicity against human ductal breast carcinoma cells T47D. *Journal of Environmental Chemical Engineering, 2*(4), 2037-2044.

Murugan, K., Benelli, G., Panneerselvam, C., Subramaniam, J., Jeyalalitha, K., Dinesh, D., . . . Madhiyazhagan, P. (2015). Cymbopogon citratus-synthesized gold nanoparticles boost the predation efficiency of copepod Mesocyclops aspericornis against malaria and dengue mosquitoe. *Experimental Parasitology, 153*, 129-138.

Mafune, F., Kohno, J., Takeda, Y., & Kondow, T. (2000). Structure and Stability of Silver Nanoparticles in Aqueous Solution Produced by Laser Ablation. *J. Phys. Chem. B, 104*(35), 8333-8337.

Marsich, L., Bonifacio, A., Mandal, S., Krol, S., Beleites, C., & Sergo, V. (2012). Poly-L-lysine-Coated Silver Nanoparticles as Positively Charged Substrates for Surface-Enhanced Raman Scattering. *Langmuir, 28*, 13166−13171.

Mulvaney, P. (1996). Surface plasmon spectroscopy of nanosized metal particles. *Langmuir, 12*, 788–800.

Murray, R. G., Steed, P., & Elson, H. (1965). The location of the mucopeptide in sections of the cell wall of Escherichia coli and other gram-negative bacteria. *Can J Microbiol, 11*, 547-60.

Moor, C., Lymberopoulou, T., & Dietrich, V. J. (2001). Determination of Heavy Metals in Soils, Sediments and Geological Materials by ICP-AES and ICP-MS. *Microchimica Acta, 136*(3), 123-128.

Nelson, D., Marcato, P. D., Souza, G. I., Alves, O. L., & Esposito, E. (2007). Antibacterial effect of silver nanoparticles produced by fungal process on textile fabrics and their effluent treatment. *Journal of Biomedical Nanotechnology, 3*, 203–208.

Narayanan, K. B., & Sakthivel, N. (2008). Coriander leaf mediated biosynthesis of gold nanoparticles. *Materials Letters, 62*(30), 4588-4590.

Nickel, U., Castell, A. Z., Poppl, K., & Schneider, S. (2000). A Silver Colloid Produced by Reduction with Hydrazine as Support for Highly Sensitive Surface-Enhanced Raman Spectroscopy. *Langmuir, 16*, 9087-9091.

Niidome, Y., Nishioka, K., Kawasaki, H., & Yamada, S. (2003). Rapid synthesis of gold nanorods by the combination of chemical reduction and photoirradiation processes; morphological changes depending on the growing processes. *Chem. Commun.*, 2376-2377.

Noruzi, M., Zare, D., Khoshnevisan, K., & Davoodi, D. (2011). Rapid green synthesis of gold nanoparticles using Rosa hybrida petal extract at room temperature. *Spectrochim. Acta A Mol. Biomol. Spectrosc., 79*, 1461–1465.

Nolan, E. M., & Lippard, S. J. (2008). Tools and Tactics for the Optical Detection of Mercuric Ion. *Chem. Rev., 108*, 3443-3480.

Ojekunle, O., Ojekunle, O., Adeyemi, A., Taiwo, A., Sangowusi, O., Taiwo, A., & Adekitan, A. A. (2016). Evaluation of surface water quality indices and ecological risk assessment for heavy metals in scrap yard neighbourhoodEvaluation of surface water quality indices and ecological risk assessment for heavy metals in scrap yard neighbourhood. *SpringerPlus, 5*(1), 560.

Okitsu, K., Sharyo, K., & Nishimura, R. (2009). One-Pot Synthesis of Gold Nanorods by Ultrasonic Irradiation: The Effect of pH on the Shape of the Gold Nanorods and Nanoparticles. *Langmuir*, 7786-7790.

Ojekunle, O. Z., Ojekunle, O. V., Adeyemi, A. A., Taiwo, A. G., Sangowusi, O. R., Taiwo, A. M., & Adekitan, A. A. (2016). Evaluation of surface water quality indices and ecological risk assessment for heavy metals in scrap yard neighbourhoodEvaluation of surface water quality indices and ecological risk assessment for heavy metals in scrap yard neighbourhood. *SpringerPlus, 5*(1), 560.

PATRA, J. M., PANDA, S. S., & DHAL, N. K. (2015). A REVIEW ON GREEN SYNTHESIS OF GOLD NANOPARTICLES. *International Journal of Pharma and Bio Sciences, 6*(3), 251-261.

Pattnaik, P. (2005). Surface Plasmon Resonance. *Applied Biochemistry and Biotechnology, 126*(5), 79-92.

Philip, D., & Unni, C. (2011). Extracellular biosynthesis of gold and silver nanoparticles using Krishna tulsi (Ocimum sanctum) leaf. *Physica E, 43*, 1318-1322.

Pong, B., Elim, H. I., Chong, J., Ji, W., Trout, B. J., & Lee, J. (2007). New Insights on the Nanoparticle Growth Mechanism in the Citrate Reduction of Gold(III) Salt: Formation of the Au Nanowire Intermediate and Its Nonlinear Optical Properties. *The Journal of Physical Chemistry C*, 6281-6287.

Posthuma-Trumpie, G. A., Korf, J., & Amerongen, A. V. (2009). Lateral flow (immuno)assay: its strengths, weaknesses, opportunities and threats. A literature survey. *Analytical and Bioanalytical Chemistry, 393*(2), 569-582.

Pal, S., Tak, Y. K., & Song, J. (2007). Does the antibacterial activity of silver nanoparticles depend on the shape of the nanoparticle? A study of the gram-negative bacterium Escherichia coli. *Applied and environmental microbiology, 73*(6), 1712-1720.

Palombo, E. A., & Semple, S. J. (2001). Antibacterial activity of traditional Australian medicinal plants. *Journal of Ethnopharmacology, 77*(2), 151–157.

Prescott, L., Harley, J., & Klein, D. (2002). *Microbiology* (5th ed., Vol. 46). New York: The McGraw-Hill Companies.

Pillai, Z. S., & Kamat, P. V. (2004). What Factors Control the Size and Shape of Silver Nanoparticles in the Citrate Ion Reduction Method? *J. Phys. Chem. B, 108,* 945-951.

Rai, M., Yadav, A., & Gade, A. (2009). Silver nanoparticles as a new generation of antimicrobials. *Biotechnology advances, 27*(1), 76-83.

Riu, J., Maroto, A., & Rius, F. X. (2006). Nanosensors in environmental analysis. *Abstract Talanta, 69*, 288-301.

Raffi, M., Hussain, F., Bhatti, T. M., Akhter, J. I., Hameed, A., & Hasan, M. M. (2008). Antibacterial Characterization of Silver Nanoparticles against. *J. Mater. Sci. Technol.*, 192-196.

Rai, A., Prabhune, A., & Perry, C. C. (2010). Antibiotic mediated synthesis of gold nanoparticles with potent antimicrobial activity and their application in antimicrobial coatings. *J. Mater. Chem.*, 6789-6798.

Ramnani, S., Biswal, J., & Sabharwal, S. (2007). Synthesis of silver nanoparticles supported on silica aerogel using gamma radiolysis. *Radiation Physics and Chemistry, 76*(8-9), 1290-1294.

Raveendran, P., Fu, J., & Wallen, S. L. (2003). Completely "Green" Synthesis and Stabilization of Metal Nanoparticles. *J. Am. Chem. Soc., 125*(46), 13940-13941.

Roe, D., Karandikar, B., Bonn-Savage, N., Gibbins, B., & Roullet, J. (2008). Antimicrobial surface functionalization of plastic catheters by silver nanoparticles. *J. Antimicrob. Chemother.*, 869-876.

Sambhy, V., MacBride, M. M., Peterson, B. R., & Sen, A. (2006). Silver Bromide Nanoparticle/Polymer Composites: Dual Action Tunable Antimicrobial Materials. *J. AM. CHEM. SOC., 128*, 9798-9808.

Shi, W., & Ma, Z. (2010). Amperometric glucose biosensor based on a triangular silver nanoprisms/chitosan composite film as immobilization matrix. *Biosensors and Bioelectronics, 26*, 1098-1103.

Shi, Z., Tang, J., Chen, L., Yan, C., Tanvir, S., Anderson, W. A., . . . Tam, K. C. (2015). Enhanced colloidal stability and antibacterial performance of silver nanoparticles/cellulose nanocrystal hybrids. *Journal of Materials Chemistry B*, 603-611.

Shirtcliffe, N., Nickel, U., & Schneider, S. (1999). Reproducible Preparation of Silver Sols with Small Particle Size Using Borohydride Reduction: For Use as Nuclei for Preparation of Larger Particles. *Journal of Colloid and Interface Science, 211*, 122-129.

Solomon, S. D., Bahadory, M., Jeyarajasingam, A. V., Rutkowsky, S. A., & Boritz, C. (2007). Synthesis and Study of Silver Nanoparticles. *Journal of Chemical Education, 84*(2), 322-325.

Sun, Y., & Xia, Y. (2002). Shape-Controlled Synthesis of Gold and Silver Nanoparticles. *SCIENCE, 298*(13).

Sarkar, J., Kalyan, S., Laskar, A., Chattopadhyay, D., & Acharya, K. (2013). Bioreduction of chloroaurate ions to gold nanoparticles by culture l filtrate of Pleurotus sapidus que. *Mater. Lett., 92*, 313-316.

Sau, T. K., Pal, A., Jana, N., Wang, Z., & Pal, T. (2001). Size Controlled Synthesis of Gold Nanoparticles using Photochemically Prepared Seed Particles. *Journal of Nanoparticle Research, 3*(4), 257-261.

Sharma, B., Dhar, D., Hazra, S., & Gogoi, L. (2014). Biosynthesis of gold nanoparticles using a freshwater green alga, Prasiola crispa. *Mater. Lett., 116*, 94-97.

Shellaiah, M., Simon, T., Suna, K. W., & Ko, F. (2015). Simple bare gold nanoparticles for rapid colorimetric detection of Cr3+ ions in aqueous medium with real sample applications. *Sensors and Actuators B: Chemical*, 44-51.

Shena, M., Du, Y., Hua, N., & Yang, P. (2006). Microwave irradiation synthesis and self-assembly of alkylamine-stabilized gold nanoparticles. *Powder Technology, 162*(1), 64-72.

Shi, W., & Ma, Z. (2010). Amperometric glucose biosensor based on a triangular silver nanoprisms/chitosan composite film as immobilization matrix. *Biosensors and Bioelectronics, 26*, 1098-1103.

Shirtcliffe, N., Nickel, U., & Schneider, S. (1999). Reproducible Preparation of Silver Sols with Small Particle Size Using Borohydride Reduction: For Use as Nuclei for Preparation of Larger Particles. *Journal of Colloid and Interface Science, 211*, 122-129.

Silva, J. N., Saade, J., Farias, P. M., & Falcão, E. H. (2013). Colloidal Synthesis of Silver Nanoprisms in Aqueous Medium: Influence of Chemical Compounds in UV/Vis Absorption Spectra. *Advances in Nanoparticles*, 217-222.

Srinath, B., & Rai, V. R. (2015). Rapid biosynthesis of gold nanoparticles by Staphylococcus epidermidis: Its characterisation and catalytic activity. *Materials Letters, 146*, 23-25.

Sudeep, P. K., & Kamat, P. V. (2005). Photosensitized Growth of Silver Nanoparticles under Visible Light Irradiation: A Mechanistic Investigation. *Chem. Mater., 17*(22), 5404-5410.

Suresh, A. K., Pelletier, D. A., Wang, W., Broich, M. L., Moon, J., Gu, B., . . . Doktycz, M. J. (2011). Biofabrication of discrete spherical gold nanoparticles using the metal-reducing bacterium Shewanella oneidensis. *Acta Biomaterialia, 7*, 2148-2152.

Sharma, A., Katnoria, J. K., & Nagpal, A. K. (2016). Heavy metals in vegetables: screening health risks involved in cultivation along wastewater drain and irrigating with wastewater. *SpringerPlus, 5*(1), 560.

Schmidt, M., Karakassopoulos, A., Burkhart, J., Deitenbeck, R., Asmus, J., Müller, T. H., . . . Walther-Wenke, G. (2007). Comparison of three bacterial detection methods under routine conditions. *Vox Sanguinis, 92*, 15–21.

Sun, Y., & Xia, Y. (2002). Shape-Controlled Synthesis of Gold and Silver Nanoparticles. *SCIENCE, 298*(5601), 2176-2179.

Tahir, K., Nazir, S., Li, B., Khan, A. U., Khan, Z. U., Gong, P. Y., . . . Ahmad, A. (2015). Nerium oleander leaves extract mediated synthesis of gold nanoparticles and its antioxidant activity. *Materials Letters, 156*, 198-201.

Tamuly, C., Hazarika, M., & Bordoloi, M. (2013). Biosynthesis of Au nanoparticles by Gymnocladus assamicus and its catalytic activity. *Materials Letters, 108*, 276-279.

Tsuji, M., Matsumoto, K., Jiang, P., Matsuo, R., Hikino, S., Tang, X., & Kamarudin, K. S. (2008). The Role of Adsorption Species in the Formation of Ag Nanostructures by a Microwave-Polyol Route. *Bull. Chem. Soc. Jpn., 81*(3), 393-400.

Turkevich, J., Stevenson, P. C., & Hillier, J. (1951). A STUDY OF THE NUCLEATION AND GROWTH PROCESSES IN THE SYNTHESIS OF COLLOIDAL GOLD. *Discuss, Faraday Soc.*, 55-75.

Vertelov, G., Krutyakov, Y., Efremenkova, O., Olenin, A., & Lisichkin, G. (2008). A versatile synthesis of highly bactericidal Myramistin® stabilized silver nanoparticles. *Nanotechnology*, 19.

Vetchinkina, E. P., Loshchinina, E. A., Burov, A. M., Dykman, L. A., & Nikitina, V. E. (2014). Enzymatic formation of gold nanoparticles by submerged culture of the basidiomycete Lentinus edodes. *J. Biotechnol., 183*, 37-45.

Varner, K. E., El-Badawy, A., Feldhake, D., & Venkatapathy, R. (2010). *State of the Science Literature Review: Everything Nanosilver and More.* U.S. Environmental Protection Agency. Washington, DC: EPA.

Wang, F., & Liu, J. (2014). Liposome Supported Metal Oxide Nanoparticles: Interaction Mechanism, Light Controlled Content Release, and Intracellular Delivery. *Small, 10*, 3927-3931.

World Health Organisation. (2011). *Guidelines for Drinking-Water Quality.* Retrieved from World Health Organisation: http://www.who.int/water_sanitation_health/publications/dwq-guidelines-4/en/

Wang, G., Zhu, X., Jiao, H., Dong, Y., & Li, Z. (2012). Ultrasensitive and dual functional colorimetric sensors for mercury (II) ions and hydrogen peroxide based on catalytic reduction property of silver nanoparticles. *Biosensors and Bioelectronics*, 337-342.

Wang, Y., Yang, F., & Yang, X. (2010). Colorimetric detection of mercury(II) ion using unmodified silver nanoparticles and mercury-specific oligonucleotides. *ACS Appl. Mater. Interfaces,*, 339-342.

Wu, J., Li, L., Zhu, D., He, P., Fang, Y., & Cheng, G. (2011). Colorimetric assay for mercury (II) based on mercury-specific deoxyribonucleic acid-functionalized gold nanoparticles. *Anal. Chim. Acta*, 115-119.

Xia, H., Ba, S., Hartmann, J., & Wang, D. (2010). Synthesis of Monodisperse Quasi-Spherical Gold Nanoparticles in Water via Silver(I)-Assisted Citrate Reduction. *Langmuir, 26*(5), 3585-3589.

Xia, Y., & Halas, N. J. (2005). Shape-Controlled Synthesis and Surface Plasmonic Properties of Metallic Nanostructures. *MRS BULLETIN, 30*, 338-348.

Xia, Y., Xiong, Y., Lim, B., & Skrabalak, S. E. (2008). Shape-Controlled Synthesis of Metal Nanocrystals: Simple Chemistry Meets Complex Physics? *A Journal of the Gesellschaft Deutscher Chemiker, 48*(1), 60-103.

Xie, J., Lee, J. Y., Wang, D. I., & Ting, Y. P. (2007). Silver Nanoplates: From Biological to Biomimetic Synthesis. *ACS Nano, 1*(5), 429-439.

Yang, N., Li, W., & Hao, L. (2014). Biosynthesis of Au nanoparticles using agricultural waste mango peel extract and its in vitro cytotoxic effect on two normal cells. *Materials Letters, 134*, 67-70.

Yao, Y. T. (2010). Cooperative Binding of Bifunctionalized and Click-Synthesized Silver Nanoparticles for Colorimetric Co2+ Sensing. *ACS Applied Materials & Interfaces*, 684-690.

Zhang, Y., Peng, H., Huang, W., Zhou, Y., & Yan, D. (2008). Facile preparation and characterization of highly antimicrobial colloid Ag or Au nanoparticles. *Journal of Colloid and Interface Science, 325*(2), 372-376.

Zhou, Y., Wang, C. Y., Zhu, Y. R., & Chen, Z. Y. (1999). A Novel Ultraviolet Irradiation Technique for Shape-Controlled Synthesis of Gold Nanoparticles at Room Temperature. Chem. Mater., 11(9), 2310-2312.

Zhao, G., & Stevens, S. E. (1998). Multiple parameters for the comprehensive evaluation of the susceptibility of Escherichia coli to the silver ion. *BioMetals, 11*, 27-32.

Appendix

Lateral Flow Biosensor: Gold & Silver Nanoparticles for Detecting Bacteria in Domestic Water

A.1 Background

Pathogens in domestic drinking water are one of the most significant reasons for human illness. In 2008, over two million people died because of diarrheal diseases caused by polluted water (Bridle, Balharry, Gaiser, & Johnston, 2015). There are mainly three kinds of microbial contamination in water: viruses, parasites, and bacteria. Most of these microbes can easily infect both humans and animals, and are also able to migrate between human and animals. Therefore, to ensure the quality of domestic drinking water, detecting and monitoring pathogens in drinking water is a necessary step. However, the current challenges of bacterial detection are either a long analysis time (typically 1-7 days), or lack of accuracy, which needs large samples to identify microbes (Schmidt, et al., 2007). Therefore, it is important to find an approach that is cheap, quick, sensitive, and easy to use to be able to detect various microbes. The unique properties of some nano-materials make them a candidate for this purpose.

In this work, bacteria in domestic drinking water are the main targets for detection purposes. Gold and silver nanoparticles are used as the agent to measure the amount of bacteria in a sample solution. The most dramatic advantage of gold and silver nanoparticles is their surface plasmon resonance, which allows gold and silver nanoparticles to change color when they are aggregated

(Lee & El-Sayed, 2006). Gold nanoparticles in water have pink or red colors, and silver nanoparticles have various colors, such as yellow, green, blue, purple, etc., depending on their size and shape. In this work, lateral flow assay (LFA) was used for bacterial detection. LFAs is prefabricated strips served as a carrier material containing dry reagents that could be activated by applying the fluid sample (Posthuma-Trumpie, Korf, & Amerongen, 2009).

A.2 Methods

Gold nanoparticles were synthesized with the method provided by the research of Nikhil et al. (Jana, Gearheart, & Murphy, 2001), and AuNPs are used as a strong catalyst (Haruta, 2002). In this work, Poly-(ethyleneimine) (PEI) was used as a weak reducing agent, which can only reduce silver ions when a catalyst is present.

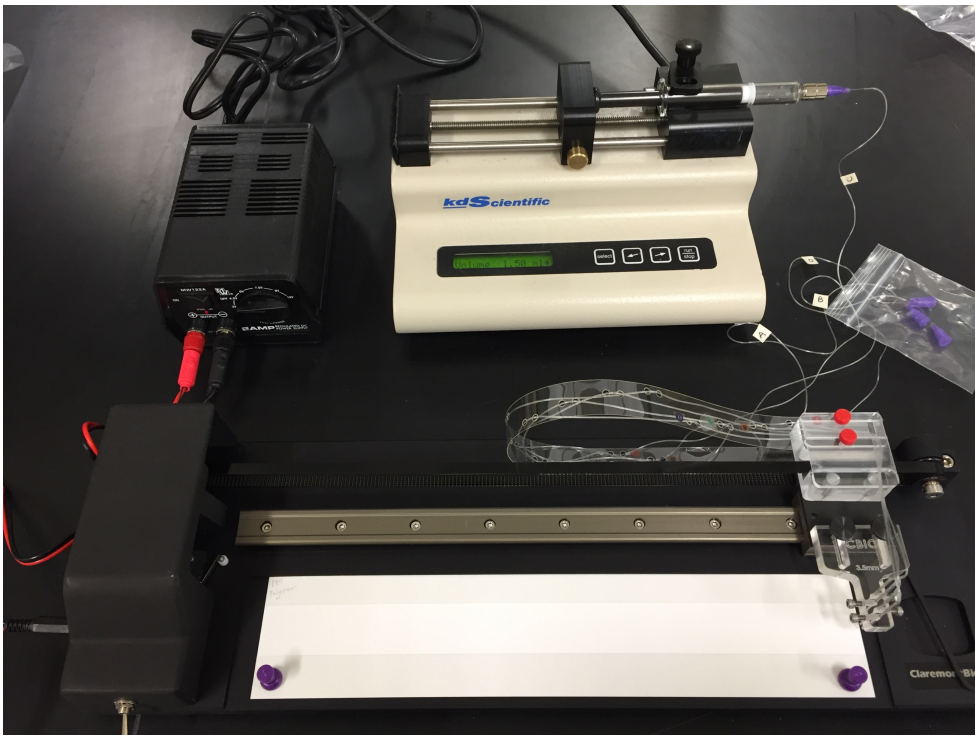

Figure A.1 Photograph of line printer with syringe pump, used for laying down a line of

reagents on lateral flow membranes.

The lateral flow strip was prepared by an line printer (Figure A.1). Three lines were printed on the membrane: (a) one was the PEI test line in the middle of the membrane, (b) an $AgNO_3$ line was printed five millimeters away from the PEI test line to the gold conjugate pad, (c) a $NaBH_4$ control line was printed between the PEI line and absorbent pad. The color changes associated with the gold and silver nanoparticles can be used in this assay method to detect the presence of microbial contamination by the appearance of colored lines on the membrane strip. The mechanisms of this reaction are shown in Figure A.2, where a sample is applied to the sample pad, and then the sample solution flows through the gold conjugated pad, the $AgNO_3$ line, the PEI line, and the $NaBH_4$ line, and is then absorbed by the absorbent pad at the end.

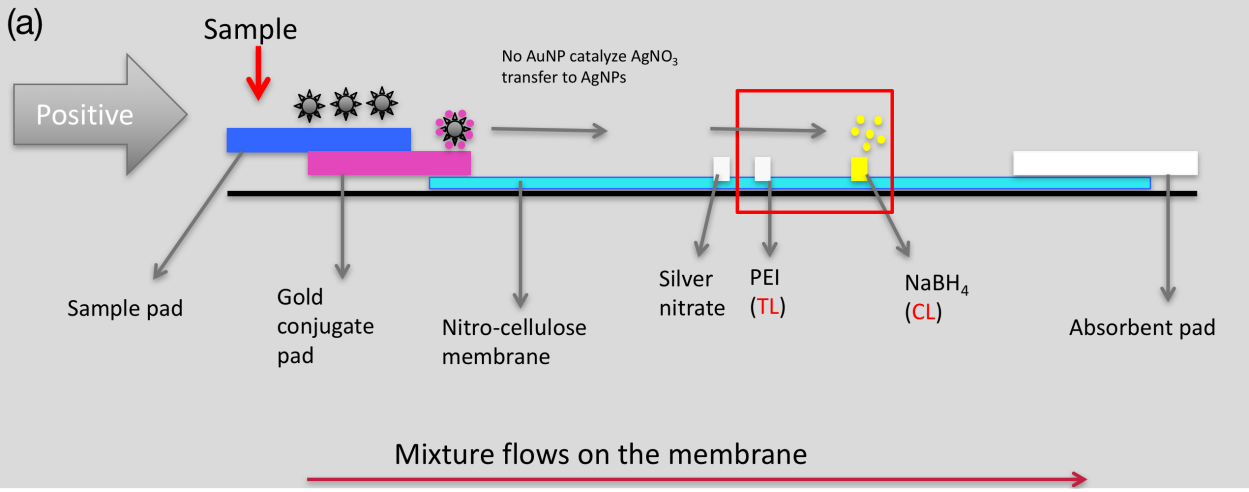

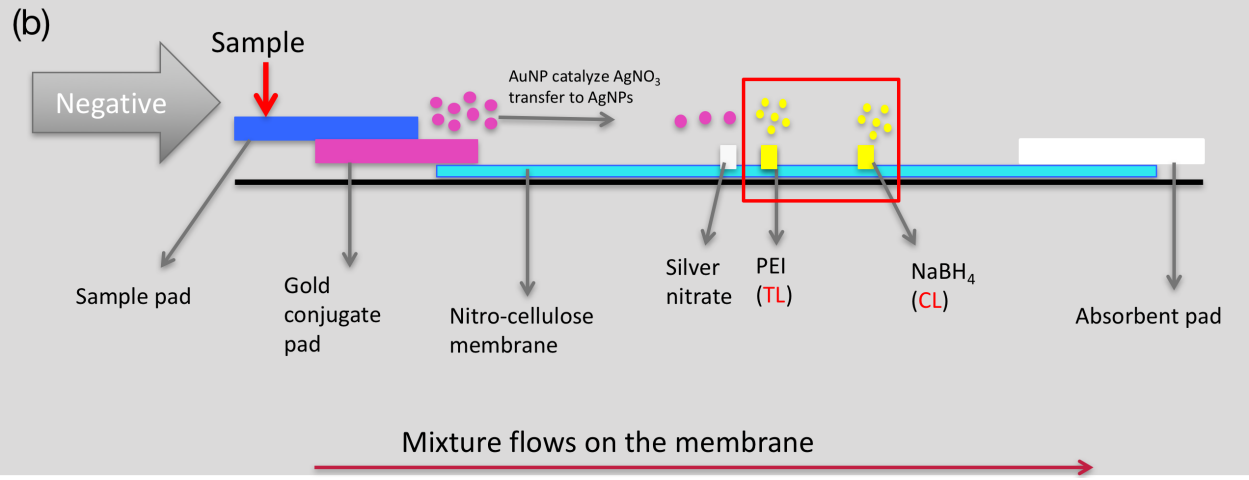

Figure A.2 Mechanisms of the lateral flow assay: (a) A positive reaction should show one yellow line on the membrane. (b) a negative reaction (sample with few or no bacteria) should show two yellow line (test line and control line) on the membrane.

Based on this design, a positive reaction should only show one yellow line on the membrane, which is the control line. Since bacteria can cause the aggregation of AuNPs and make them stay on the conjugate pad, thereby there should no reaction happening when the solution flows through the $AgNO_3$ line and PEI line, and thus, only the control line would give a yellow color. On the other hand, a negative reaction (i.e. a sample with few or no bacteria compare to the detection limited), should show two yellow lines (test line and control line) on the membrane. Two lines would occur when the sample solution flows through the gold conjugate pad where there are spare available AuNPs that can catalyze the reaction between the $AgNO_3$ line and PEI line. This method potentially saves time, is accurate, and may be suitable for domestic drinking water monitoring.

A.3 Results

For this study, the PEI test line was observed after applying a bacterial solution to the membrane. However, in this work, the $AgNO_3$ line and $NaBH_4$ line were not long lasting when exposed to air. Sometimes the $AgNO_3$ could reduce and change color by air, and when the sample solution flowed to the control line, there was no color changed. In addition, AuNPs were easily lost their activity after drying on the conjugated pad, presumably due to aggregation that was not easily reversible.

A.4 Conclusions and Recommendations

The chemical method lateral flow assay using silver and gold nanoparticles was unsuccessful. This might be due to the oxygen in the air causing $NaBH_4$ oxidation. To solve this problem, a sealed apparatus should be developed for this assay. Furthermore, gold nanoparticles processing should be improved to keep their activity after drying on the conjugated pad, or by minimizing drying.